

N-Doped Mesoporous Carbon Supported Dual-Metal Atom M-N-C Desert Rose Structure as An Effective Bifunctional Electrocatalyst for Zinc-Air Battery



By

Uswa Arooj

(Registration No: 00000403073)

Department of Energy Systems Engineering

US-Pakistan Centre for Advanced Studies in Energy (USPCAS-E)

National University of Sciences & Technology (NUST)

Islamabad, Pakistan

(2024)

**N-Doped Mesoporous Carbon Supported Dual-Metal Atom M-
N-C Desert Rose Structure as An Effective Bifunctional
Electrocatalyst For Zinc-Air Battery**



By

Uswa Arooj

(Registration No: 00000403073)

A thesis submitted to the National University of Sciences and Technology, Islamabad,

in partial fulfillment of the requirements for the degree of

Master of Science in

Energy Systems Engineering

Supervisor: Dr. Naseem Iqbal

US-Pakistan Centre for Advanced Studies in Energy (USPCAS-E)

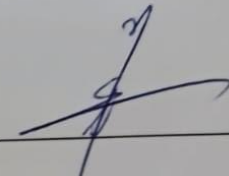
National University of Sciences & Technology (NUST)

Islamabad, Pakistan

(2024)

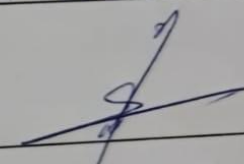
THESIS ACCEPTANCE CERTIFICATE

Certified that the final copy of MS Thesis written by Ms Uswa Arooj (Registration No. 00000403073), of ESE, USPCASE has been vetted by the undersigned, found complete in all respects as per NUST Statutes/ Regulations/ Masters Policy, is free of plagiarism, errors, and mistakes and is accepted as partial fulfilment for the award of Master's degree. It is further certified that necessary amendments as pointed out by GEC members and foreign/ local evaluators of the scholar have also been incorporated in the said thesis.

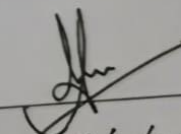
Signature: _____ 

Name of Supervisor Dr. Naseem Iqbal

Date: 06-01-2025

Signature (HOD): _____ 

Date: 06-01-2025

Signature (Dean/ Principal) _____ 

Date: 14/01/2025

National University of Sciences & Technology

MASTER'S THESIS WORK

We hereby recommend that the dissertation prepared under our supervision by (Student Name & Regn No.) Usqa Arooj, 00000403073

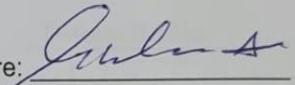
Titled: N-Doped mesoporous carbon supported dual metal atom M-N for oxygen electrode electro catalyst in zinc air batteries in partial fulfillment of the requirements for the award of MS Energy Systems Engineering degree with (A grade).

Examination Committee Members

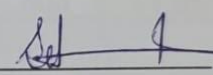
1. Name Dr. Nadia Shahzad

Signature: 

2. Name Dr. Ghulam Ali

Signature: 

3. Name Dr. Sehar Shakir

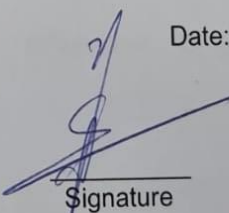
Signature: 

Supervisor's name: Dr. Naseem Iqbal

Signature: 

Date: 23-12-2024

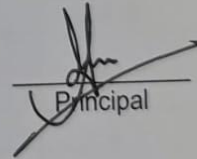
Head of Department


Signature

23-12-2024
Date

COUNTERSIGNED

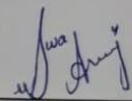
Date: 14/01/2025


Principal

CERTIFICATE OF APPROVAL

This is to certify that the research work presented in this thesis, entitled “**N-doped mesoporous carbon supported Dual-metal atom M-N-C desert rose structure as an effective Bifunctional electrocatalyst for zinc-air battery**” was conducted by Mr./Ms. Uswa Arooj under the supervision of Dr. Naseem Iqbal. No part of this thesis has been submitted anywhere else for any other degree. This thesis is submitted to the US-Pakistan Centre for Advanced Studies in Energy (USPCASE) in partial fulfilment of the requirements for the degree of Master of Science in the Field of Energy Systems Engineering Department of USPCASE National University of Sciences and Technology, Islamabad.

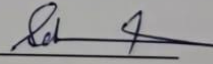
Student Name: Uswa Arooj

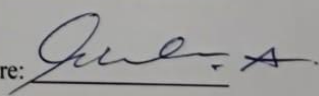
Signature: 

Examination Committee:

- a) GEC Member 1: Dr. Nadia Shahzad
(Associate Professor, ESE, USPCAS-E)
- b) GEC Member 2: Dr. Sehar Shakir
(Assistant Professor, ESE, USPCAS-E)
- c) GEC Member 3: Dr. Ghulam Ali
(Associate Professor, ESE, USPCAS-E)

Signature: 


Signature: 

Signature: 

Supervisor Name: Dr. Naseem Iqbal

Signature: 

Name of HOD: Dr. Naseem Iqbal

Signature: 

Name of Principal/Dean: Dr. Adeel Waqas

Signature: 

AUTHOR'S DECLARATION

I Uswa Arooj hereby state that my MS thesis titled "**N-doped mesoporous carbon supported Dual-metal atom M-N-C desert rose structure as an effective Bifunctional electrocatalyst for zinc-air battery**" is my work and has not been submitted previously by me for taking any degree from the National University of Sciences and Technology, Islamabad or anywhere else in the country/ world.

At any time if my statement is found to be incorrect even after I graduate, the university has the right to withdraw my MS degree.

Name of Student: Uswa Arooj

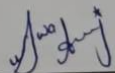
Date: 06-01-2025

PLAGIARISM UNDERTAKING

I solemnly declare that the research work presented in the thesis titled "**N-doped mesoporous carbon supported Dual-metal atom M-N-C desert rose structure as an effective Bifunctional electrocatalyst for zinc-air battery**" is solely my research work with no significant contribution from any other person. Small contribution/ help wherever taken has been duly acknowledged and that complete thesis has been written by me.

I understand the zero-tolerance policy of the HEC and the National University of Sciences and Technology (NUST), Islamabad towards plagiarism. Therefore, I as an author of the above-titled thesis declare that no portion of my thesis has been plagiarized and any material used as reference is properly referred/cited.

I undertake that if I am found guilty of any formal plagiarism in the above-titled thesis even after the award of MS degree, the University reserves the right to withdraw/revoke my MS degree and that HEC and NUST, Islamabad have the right to publish my name on the HEC/University website on which names of students are placed who submitted plagiarized thesis.

Student Signature:  _____

Name: _____ Uswa Arooj _____

DEDICATION

"This work is dedicated to my loving **parents**, Asif Hussain and Zaheera Rauf who have always been my greatest source of strength and motivation. Their constant support, love, and belief in me have carried me through every challenge. I wouldn't have made it this far without them.

I also dedicate this work to myself, for the perseverance, resilience, and determination that guided me through challenges and kept me focused on achieving my goals throughout this journey."

ACKNOWLEDGEMENTS

I humbly thank Allah Almighty, the Most Compassionate and Merciful, for His endless blessings, including the health, strength, and resilience to pursue my academic journey.

I am deeply grateful to **Dr. Naseem Iqbal**, my research supervisor, for his constant support, invaluable guidance, and inspiring mentorship. His encouragement and patience have been a source of strength, helping me overcome challenges and grow both personally and professionally. I sincerely appreciate the time and effort he has invested in my journey, and I feel truly fortunate to have had such an exceptional mentor.

I am also grateful to my GEC members, Dr. Nadia Shahzad, Dr. Sehar Shakir, and Dr. Ghulam Ali, for their guidance and support. I would also like to express my gratitude to my previous teachers, whose guidance and encouragement laid the foundation for my academic journey and inspired me to reach new heights.

Special thanks to Dr. Rimsha Mehek and Dr. Neelam Zaman for their unwavering support, kind guidance, and invaluable contributions throughout my research journey.

I am especially grateful to Ms. Rimsha Mehek for her dedicated assistance with electrochemical testing, which significantly enriched my work. I also extend my sincere thanks to Dr. Adeel Waqas, Principal of USPCAS-E, for fostering a supportive and inspiring research environment. My heartfelt appreciation goes to the faculty and lab staff of USPCAS-E, especially Sir Naveed Ahmed, for his constant help and support in various lab matters, which greatly facilitated my research.

I am profoundly thankful to my wonderful parents for their endless love and support, and to my amazing siblings for their constant encouragement and belief in me, which have been a source of strength and inspiration throughout this journey. A special thanks to my sister, Maleeka Bakhtawar, for her invaluable support in providing research articles and her steadfast motivation during challenging times. I also extend my heartfelt gratitude to my friends Hamna, Jaria, Tooba, Warda and Haleema for their kindness and encouragement, which made this journey more meaningful. Additionally, I am thankful to my all-lab fellows for their invaluable support and cooperation, which greatly contributed to my research experience.

TABLE OF CONTENTS

ACKNOWLEDGEMENTS	VIII
TABLE OF CONTENTS	X
LIST OF TABLES	XIII
LIST OF FIGURES	XIV
LIST OF SYMBOLS, ABBREVIATIONS AND ACRONYMS	XV
ABSTRACT	XVI
CHAPTER 1: INTRODUCTION	1
1.1 Background	1
1.2 Conventional Energy Storage Methods	3
1.3 Alternative Energy Storage Methods	3
1.4 Metal-Air Batteries	4
1.5 Types of Metal-Air Batteries	5
<i>1.5.1 Zinc-Air Batteries</i>	<i>7</i>
1.6 Bifunctional Electrocatalysts for RZABs	10
1.7 Advancements in Material Developments	11
<i>1.7.1 Single Atom Catalyst</i>	<i>12</i>
<i>1.7.2 Dual Atom Catalyst</i>	<i>14</i>
1.8 Problem Statement	16
1.9 Research Objectives	17
CHAPTER 2: LITERATURE REVIEW	18
2.1 Research gap	22
2.2 Purposed Solutions	23
CHAPTER 3: INTRODUCTION TO EXPERIMENTAL TECHNIQUES	24
3.1 Physical Characterizations	24
3.2 Electrochemical Characterization	28
CHAPTER 4: METHODOLOGY	30
4.1 Material Collection and Methods	30
<i>4.1.1 Material Collection</i>	<i>30</i>
<i>4.1.2 Synthesis of Mn-N-C/N-MC</i>	<i>30</i>
<i>4.1.3 Synthesis of Co-N-C/N-MC</i>	<i>30</i>
<i>4.1.4 Synthesis of Co Mn-N-C/N-MC</i>	<i>31</i>
CHAPTER 5: RESULTS AND DISCUSSION	32
5.1 X-Ray Diffraction (XRD)	32

5.2 Scanning Electron Microscopy	33
5.4 Raman Spectroscopy	35
5.5 X-Ray Photoelectron Spectroscopy (XPS)	36
5.6 Linear Sweep Voltammetry (LSV)	38
5.6.1 <i>Oxygen Reduction Reaction (ORR)</i>	38
5.6.2 <i>Oxygen Evolution reaction (OER)</i>	39
5.7 Stability Test	42
5.8 Electrochemical Impedance Spectroscopy	43
CHAPTER 6: CONCLUSION AND FUTURE RECOMMENDATION	46
6.1 Conclusion	46
6.2 Future Recommendation	46
LIST OF PUBLICATIONS	55

LIST OF TABLES

Table 5. 1 Electrochemical performance Prepared sample.....	41
Table 5. 2 Comparison with Literature	42
Table 5. 3 Charger transfer resistance of each sample	44

LIST OF FIGURES

Figure 1. 1 Energy Storage Devices [9]	2
Figure 1. 2 Recent advances on Metal-air batteries [31]	6
Figure 1. 3 Theoretical energy density of different metal-air batteries [21]	7
Figure 1. 4 Schematic of a zinc-air battery showing its structure, operation in aqueous and solid-state systems [35]	9
Figure 1. 5 Diagram of standard commercial cathodes used in zinc-air batteries [38]	10
Figure 1. 6 Illustrates the basic requirements for a bifunctional catalyst	11
Figure 1. 7 SAC Applications Overview [50]	14
Figure 1. 8 DAC Types and Applications Overview [49]	15
Figure 2. 1 a) Schematic illustration for the synthesis of Fe-NC/rOCNT hybrids. b) TEM image of Fe-ZIF/OCNT. c) SEM image. d) TEM image of Fe-NC/rOCNT. e) EDS mapping of Fe-NC/rOCNT. f) HAADF-STEM image of Fe-NC/rOCN.....	20
Figure 3. 1 A schematic of X ray diffraction	24
Figure 3. 2 The Bragg's Law [11]	25
Figure 3. 3 Illustration of how SEM works [72]	26
Figure 3. 4 Working principle of XPS [5]	27
Figure 3. 5 Nyquist plot and its corresponding equivalent circuit, illustrating the influence of diffusive impedance [84]	29
Figure 4. 1 Schematic representation of Co Mn-N-C/MC.....	31
Figure 5. 1 XRD pattern of Co-N-C/N-MC, Mn-N-C/N-MC Co Mn-N-C/N-MC...33	33
Figure 5. 2 SEM images of Co Mn-N-C/MC (a) After pyrolysis (b) After acid itching	34
Figure 5. 3 BET analysis (a) N ₂ -sorption isotherms of CoMn-N-C/N-MC, (b) pore size distribution CoMn-N-C/N-MC	35
Figure 5. 4 Raman spectra of Co Mn-N-C/N-MC, Mn-N-C/N-MC, Co-N-C/N-MC	36
Figure 5. 5 (a)XPS spectrum of Co Mn-N-C/N-MC (b) C1s (c) N1s (d)Co 2p (e) O1s (f) F1s.....	38
Figure 5. 6 (a) ORR of Co-N-C/N-MC, Co-N-C/N-MC, Co Mn-N-C/N-MC and 10% Pt/C (b) ORR at different rpm (c) K-L plots (d) OER plots Co-N-C/N-MC, Co-N-C/N-MC, Co Mn-N-C/N-MC and RuO ₂ (e) Tafel plots (f) Combined ORR and OER overall LSV curves of Co Mn-N-C/N-MC.....	40
Figure 5. 7 Stability curve (a) OER and (b) ORR	43
Figure 5. 8 EIS plots of Co-N-C/N-MC, Mn-N-C/N-MC and Co Mn-N-C/N-MC .44	44

LIST OF SYMBOLS, ABBREVIATIONS AND ACRONYMS

MAB	Metal Air battery
ZAB	Zinc Air Battery
ORR	Oxygen reduction reaction
OER	Oxygen evolution reaction
SAC	Single metal atom catalyst
DAC	Dual metal atom catalysts
XRD	X-Ray Diffraction
SEM	Scanning electron microscopy
BET	Brunauer-Emmett-Teller
TEM	Transmission electron microscopy
XPS	X-ray photoelectron spectroscopy
2MI	2-methylimidazole
MNC	Metal nitrogen carbon
N-MC	Nitrogen doped mesoporous carbon

ABSTRACT

Zinc-air batteries emerge as a highly promising option for renewable energy storage within grid systems and electric vehicles amidst global warming and energy scarcity. However, challenges such as sluggish kinetics of oxygen evolution reaction & oxygen reduction reaction have hindered their large-scale commercialization. This study addresses these challenges by developing a bifunctional oxygen electrocatalyst utilizing cobalt-manganese nitrogen-doped mesoporous carbon (Co-Mn/N-MC) using a template casting method. Bimetallic catalysts offer improved catalytic activity by leveraging the complementary properties of both cobalt and manganese within a nitrogen-doped carbon framework. The Co-Mn/N-MC catalyst demonstrated impressive results for both key reactions. For ORR, it achieved a half-wave potential ($E_{1/2}$) of 0.85 V, reflecting high activity. Regarding the OER it showed an over potential of 360mV at 10mA/cm² and a Tafel slope of 55 mV/dec, indicating efficient reaction kinetics. This research demonstrates a scalable and cost-effective catalyst with performance comparable to traditional catalyst based on precious metal such as iridium and platinum by using abundant, low-cost materials, the proposed catalyst addresses key economic and technical barriers to the commercialization of MABs. With enhanced bifunctional performance, this study contributes to the broader implementation of metal air batteries in grid scale energy storage, electric vehicle and other renewable energy systems.

Keywords: *Accessible active site; Mesoporous carbon; Oxygen reduction reaction; Dual-atom electrocatalyst; Zinc-air battery*

CHAPTER 1: INTRODUCTION

1.1 Background

No-renewable energy resources are finite sources that release harmful gases such as methane and carbon dioxide into the atmosphere. These emissions significantly contribute to global warming & continuous rise in Earth's temperature. The entire ecosystem is being disrupted by excessive global warming, including humans, wildlife, and marine life [1],[2]. This has prompted extensive study into renewable and environmentally friendly energy sources, which include hydropower, photovoltaics, wind turbines and solar. Solar and wind energy rely on weather conditions that have unpredictable and erratic qualities. To harness these sustainable energy sources ,advanced energy storage systems must be developed .Such a system can address peaks demands reducing grid stress and mitigating price surges[3],[4]. Various energy storage methods such as electrochemical ,mechanical thermal and other are viable solutions[5],[6]. Among these systems batteries are favored due to their rapid charge discharge capabilities compared to turbines and engines. Examples of such batteries include lead acid battery, lithium , sodium Sulphur , lithium ion metal-air, nickel-cadmium, and others [7]. Batteries, which are available in a range of sizes and forms, are among the greatest options for energy storage. The rise of electric vehicles and portable devices has created a growing demand for power sources. Lithium-ion batteries are considered a promising solution because of their superior energy density compared to other batteries. However ,the energy density of lithium ion battery is restricted by complex chemistry involved in their electrode material ,making them less suitable for practical electric vehicle application [8].

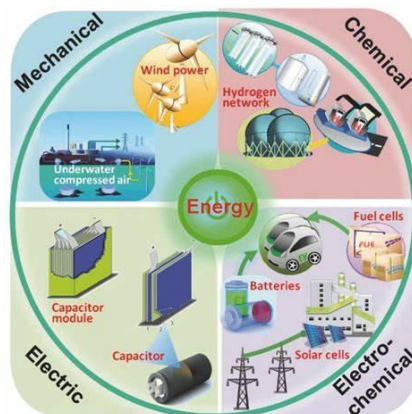


Figure 1. 1 Energy Storage Devices [9]

Metal air batteries are an emerging technology that shows suitability for electric vehicles, electronic and wearable devices. Their attractive features include high energy density, flat discharge voltage, safety of operation, simplicity of system and lower cost [10]. However, much work is still needed before substantial commercialization of such batteries can be realized. MABs can be made rechargeable if efficient bifunctional electrocatalysts are available. Many materials are explored for this purpose and precious metal-based catalysts are considered as benchmarks due to their high activities. However, they are too expensive to be employed commercially [11]. When cheap alternative materials are explored, transitional metal-based materials show good potential as bifunctional electrocatalyst [12]. Among these materials metal-nitrogen-carbon based advance material have high activity and are very promising to replace precious metal. In such catalysts metal atoms such as Co, Mn, Fe are surrounded by nitrogen atoms and anchored on carbon supports like graphene or activated porous carbon [13]. Moreover, long term stability of the catalysts has prime importance for practical applications. Several Strategies have been implemented to enhance these properties effectively. One such strategy is doping of an appropriate metal or non-metal that can provide ground for tuning majorly electronic structure and consequently reactants B.E and active sites' intermediate [14].

1.2 Conventional Energy Storage Methods

The conventional energy carriers are mainly fossil fuels like gasoline used for vehicles and stationary energy needs. Such methods are inefficient, non-sustainable and damage the environment [15]. For storage of intermittent or renewable energy, li-ion batteries are used to run PEDs and EVs. These have been very successful for PEDs but for EVs much improvement is needed to allow long distances with least interruptions [16].

1.3 Alternative Energy Storage Methods

To mitigate the challenges & surpass the limitation of conventional systems, many alternative energy storage methods are being explored to meet high demands of increasing population. Hydrogen is an emerging fuel that offers a good deal of advantages over conventional fuels. Since it can be extracted from water, circularity and sustainability are achieved by shifting to hydrogen [17]. However, one of the biggest challenges associated with hydrogen infrastructure is the storage of hydrogen. Hydrogen is a very light molecule which makes it occupy a large volume for a small mass. For practical purposes, hydrogen must be compressed and cooled down to decrease the volume. The extreme conditions of high pressure or low temperature make the storage of hydrogen unsafe and costly [18]. There have been many methods under research to allow safe hydrogen storage by absorbing in materials such as metal hydrides or metal-organic-frameworks so that hydrogen remain stable and can be released when desired by heating the materials [19].

Lithium-ion batteries have very good rechargeability and long cycle life due to which they are extensively utilized in portable electronic devices & are widely used in portable electronic devices and considered a suitable option for electric vehicles. On the other hand, LIBs are expensive, and the use of inorganic electrolytes and reactive Li makes it prone to thermal runaway raising safety concerns. Their efficiency is less than 30% which makes them not very suitable for electric vehicles [20]. To make them suitable for EVs, some features such as power density, safety and energy density need to be improved. Metal air batteries (MABs) are an emerging technology that is drawing significant interest from researchers for its high energy density. MABs can use cheaper metal as anode and safe

aqueous electrolytes make them significantly cheaper. Oxygen is received from the atmosphere; therefore, oxygen storage is not required. This makes the battery cheaper, lighter, and simpler [21] .

1.4 Metal-Air Batteries

These are electrochemical systems that is mainly consist of cathode, anode, separator & electrolyte. Anode consists of a metal that oxidizes to form metal ions while releasing electrons. A separator is a permeable membrane that allows selective ions to pass through and is a prime component to allow the functioning of cell by preserving electroneutrality.

Oxygen passes through a gas diffusion layer and enters the cathode where it is reduced by the incoming electrons. As a result, hydroxide ions are formed that is the oxygen reduction reaction. These hydroxide ions combine with the metal cations that came from anode to cathode. As an overall reaction, metals have reacted with oxygen and water to form metal hydroxides and generated useful electric current [22].

MABs are very suitable for applications where high energy densities are required, for example electric vehicles. MABs are versatile and with flat discharge voltage, they have good applicability for PEDs and grid storage. Since MABs can work with aqueous electrolytes, they resist explosions. MABs have low cost because of many reasons. Affordable & readily available metals serve as anode while oxygen functions as cathode reactant due to which oxygen storage is not required. The fabrication process is also cheap because unlike lithium, the metals can be handled under normal conditions and safety concerns are also relaxed [23].

Different types of metals can be used as anode, for example Li, Zn, Al, and Fe. Li, K, and Na are more stable in non-aqueous electrolytes, and metals like Zn, Al & Fe exhibit better aqueous` electrolyte stability. Among all MAB, zinc air batteries gained more popularity because of their rechargeability, stability and high voltage. They are employed in hearing aids and medical devices for providing a constant power for long times [24].

MABs are mostly primary batteries i.e., they cannot be recharged once the anode is consumed. However, if the electrocatalyst at cathode can drive the oxygen evolution reaction, the battery can be recharged. A catalyst that can catalyze both types of oxygen reactions is termed as a bifunctional electrocatalyst. In many studies, zinc-air batteries have shown favorable results for rechargeability. However, the secondary (rechargeable) MABs face many issues, for example formations of dendrites that lead to short circuits. Primary MABs have a relatively simplified system but the recycling infrastructure must be there to generate metals from hydroxides that have been produced during discharge process of the battery [25]. The mechanisms of ORR and OER are very different, they demand different types of active sites making it challenging to design single active site capable of catalyzing both reactions [26]. However, various design strategies are adopted to design such electrocatalyst that can incorporate both types of active sites. Such a catalyst is known as a bifunctional electrocatalyst.

1.5 Types of Metal-Air Batteries

MABs are broadly classified as those based on aqueous and non-aqueous electrolytes [27]. Metals like Zn, Mg & Al are compatible with electrolytes with aqueous solution but reactive species of metal such as Na & Li are compatible with non-aqueous solution of electrolyte. Former ones are safer because of resistance to explosions, that's why such batteries get significant attention from the scientific community. For Al-air and Zn-air batteries alkaline electrolytes like a water-based solution of potassium hydroxide are common. However, such electrolytes are also associated with a smaller voltage window because water gets decomposed into hydrogen and oxygen at voltages above 1.23 V [28]. Also, evaporation of water can alter the concentration of electrolytes that can have unwanted effects on the performance of battery.

In case of sodium and li air battery, the non-aqueous solution of electrolytes allow a wider electrochemical voltage window and high energy density [29]. However, such electrolytes have associated hazards and risk of explosion. Both aqueous and non-aqueous MABs have their own advantages and limitations, and the choices are based on the applications.

- Li Air battery
- Iron Air Battery
- Aluminum air battery
- Zinc iron battery

Li-air batteries have a very high energy density like that of gasoline. However, they have a high cost due to scarcity of lithium. Lithium is highly reactive and must be handled under controlled conditions to prevent its contact with moisture or air that consequently increases the cost even further. Now a days famous batteries such as li-ion batteris are the most successful rechargeable batteries and are employed worldwide in all types of electronic devices [30]. However, their energy density is far less than Li-air battery. The recovery and recycling of Li from such batteries is an un-resolved problem that makes these batteries not a sustainable choice.

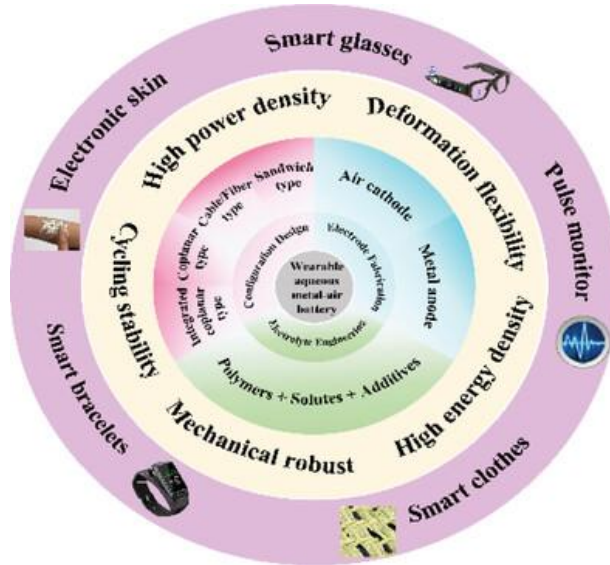


Figure 1. 2 Recent advances on Metal-air batteries [31]

Zinc air batteries are considered the most MAS because of favorable results obtained in terms of rechargeability and stability. Unlike Li, Zn is less reactive and can be handled under mild conditions. Moreover, the low cost and abundance are big advantages [32].

High Energy density such as aluminum air battery second only to Li-air battery among MABs. Al has a very safe nature, and this abundant metal is already a part of daily life in terms of food packaging, utensils, windows and so on. Al is recyclable and allows to store energy. Aluminum air batteries are not rechargeable due to which the recycling would be more frequent, and the infrastructure would be large and complicated. If Al-air batteries can be made sufficiently rechargeable, it will be a great achievement in the domain of green energy storage [33].

Iron Air battery is very interesting because of the very low cost and high abundance of Fe. Although the energy density is not lower and not very suitable for demanding applications like electric vehicles, the Fe-based battery is a great choice for stationary storage where lower energy densities are acceptable [34].

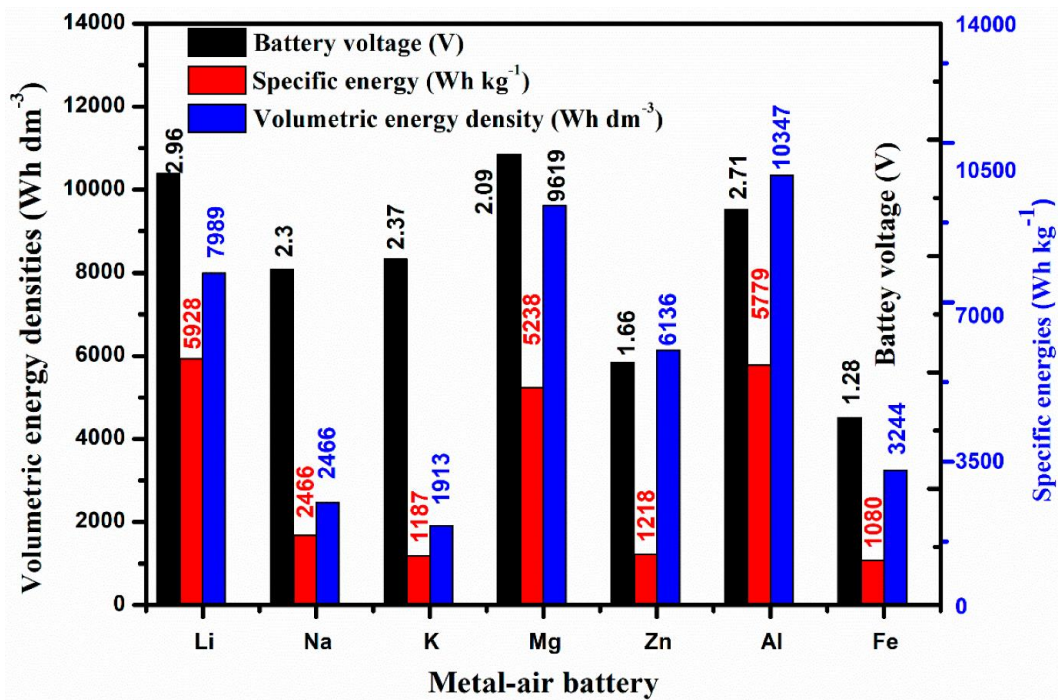


Figure 1. 3 Theoretical energy density of different MABs [21]

1.5.1 Zinc-Air Batteries

Generally, Zinc-air batteries typically consist of three primary components, an anode, cathode & electrolyte (Figure 1.4). Zn metal used as anode while cathode comprise

air electrode with a gas diffusion & catalyst layer. The whole setup is separated by porous separator immersed with solution of 6M KOH and 0.2M Zn (CH₃COO)₂ electrolyte. In detail, an electrolyte is used for transferring of OH⁻ species between cathode and anode, a physical barrier i.e. porous separator is used between both electrodes for prevention of short circuit, for improving transfer rate gas diffusion layer is applied to catalyst surface and a catalyst layer is added to increase reaction rate and kinetics. Zinc air battery is a rechargeable battery that follows redox chemistry like other batteries. During discharge process, there is oxidation on the anode side and reduction on cathode side and vice versa in charge process. There are two important reactions:

- i. Oxygen reduction reaction (ORR)
- ii. Oxygen evolution reaction (OER)

on cathode surface that completes electro chemistry of air battery. OER happens on a catalyst layer of positive electrode while battery is under charging process that corresponds to formation of O₂ from OH⁻ & oxygen utilization during ORR. Detailed charge-discharge reactions will be discussed in the working principle of zinc-air battery.

All batteries undergo charge and discharge operations. Electrochemical conversions of re-chargeable Zn-air battery are accomplished through these two processes. The following equations (equations 1.1, 1.2 and 1.3) can be used to express these discharge processes:

At Zn anode:



At air Cathode:



Overall Reaction:



All above reactions are reversed in case of charging, and the electrical energy drives the non-spontaneous chemical reactions to obtain the initial reactants. Therefore, metals deposit at anode during recharging and oxygen is released. This is called the oxygen evolution reaction (OER).

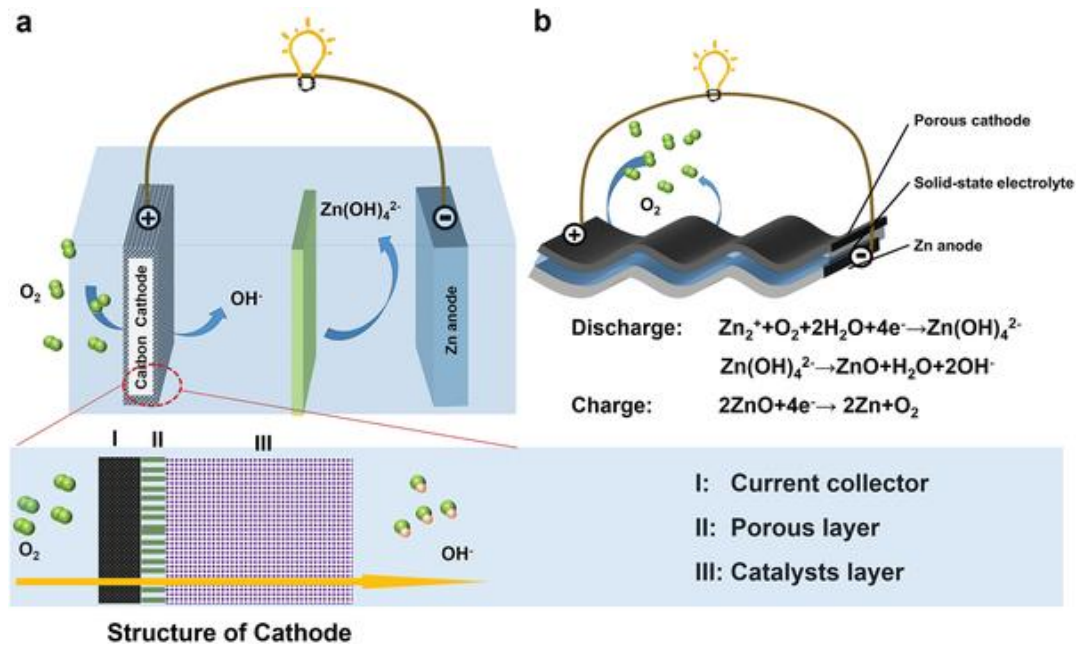


Figure 1. 4 Schematic of a zinc-air battery showing its structure, operation in aqueous and solid-state systems [35]

The sections below cover electrochemistry & engineering problems of cathode & anode in more detail.

Anode is also a major part of battery, and their understanding is also important. Zinc anode serves as energy storage component in a zinc-air cell. During discharge process 2 valence e^- are released by zinc.[36]. Research shows that zinc powder with porosity levels ranging from 60% to 80% can achieve a specific energy capacity between 1.2 and 2.2 Ah/cm² [37].

Concentrated solution of potassium hydroxide used in zinc air battery due to high ionic conductivity. During the discharge process, the zinc anode goes through several

chemical reactions, including dissolving into ions and the oxidation of its surface atoms [37]. The solubility of zinc and the types of ions formed when it dissolves depend on the pH level. For instance, insoluble compounds like ZnO (zinc oxide) and Zn(OH)₂ (zinc hydroxide) can form in solutions with a pH around 8 to 13.

Air oxygen interacts at the triple phase boundary where O₂, catalyst surface & electrolyte encounter cathode (Figure 1.5). During the discharge process, the O₂ is reduced and consumes e⁻ released at anode due to oxidation of zinc anode. The oxygen reduction reaction is slow, prompting significant research into ways to enhance this process through catalysis. Two important pathways are involved in ORR i.e. 2e⁻ pathway and 4e⁻ pathway previous one is less efficient than other. Precious metals are well-established catalysts that facilitate the four-electron pathway; however, their high cost has driven the search for alternative catalysts [37].

Cathode Designing is crucial for ensuring that oxygen can effectively diffuse to catalyst layer. Although using air O₂ is cost effective and convenient, it poses a challenge since the concentration of oxygen in air is only about 20%, and even lower when the air is fully humidified, resulting in a relatively low mass transfer driving force.

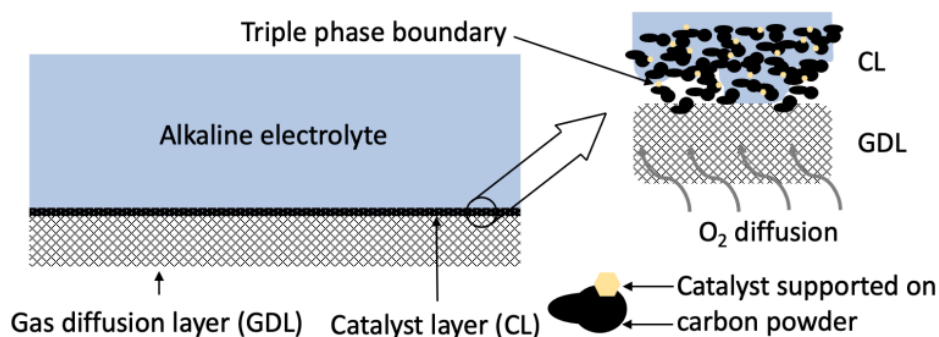


Figure 1. 5 Standard Cathodes used in metal air battery [38]

1.6 Bifunctional Electrocatalysts for RZABs

Choosing the right electrocatalyst is vital for improving a battery's electrode capacity and creating a long-lasting, efficient energy storage system. The electrocatalyst's

properties significantly affect performance and make it key factor. Bifunctional oxygen catalysts should have stability, high activity and selectivity. Figure 1.6 illustrates the bifunctional basic parameters. Bi functional electrocatalysts are increasingly preferred over monofunctional ones to improve ZAB performance. Bifunctional electrocatalysts must meet specific parameters to provide both ORR and OER activity [39].



Figure 1. 6 Illustrates the basic requirements for a bifunctional catalyst

1.7 Advancements in Material Developments

Precious metals such as ruthenium (Ru), platinum (Pt), iridium (Ir), and their alloys, have long been regarded as the standard for advanced electrocatalysts. This reputation stems from their exceptional catalytic activity in facilitating both ORR & OER. However, despite their effectiveness, the high cost of these materials has limited their widespread use and scalability in practical applications. Recent years, the focus on transition metal catalyst has significantly increased, with particular attention directed towards single atom catalyst & dual atom catalyst. These innovative materials offer a promising alternative to noble metals by leveraging the unique properties of transition metals while potentially reducing costs. SACs, which consist of individual metal atoms dispersed on a support, can provide

high catalytic activity with minimal material usage. DACs, on the other hand, incorporate pairs of metal atoms, allowing for enhanced catalytic performance through synergistic effects. The development of SACs and DACs represents a significant advancement in the field of electrocatalysis, as they not only aim to provide a more affordable solution but also maintain or even improve upon the catalytic efficiencies seen with traditional noble-metal-based materials. This shift towards transition metal catalysts is paving the way for more sustainable and economically viable electrocatalytic technologies [40-43].

1.7.1 Single Atom Catalyst

Single metal atoms are characterized by metal atoms individually dispersed on support material. The stabilization of these materials of this atomically dispersed metal atom depends on their interaction with surrounding atom. Coordination atoms can include carbon, nitrogen, sulfur, oxygen, and phosphorus, functioning similarly to the coordination atoms found in organometallic structures. Additionally, metallic supports can enhance the performance of SACs by leveraging metal-metal interactions [44].

Recent advancements in nanomaterials have facilitated the development of single-atom catalysts (SACs). The origins of this research can be traced back to the 1990s when Thomas et al. achieved the atomic dispersion of titanium (Ti) on an MCM-41 surface. This Ti catalyst exhibited exceptional selectivity in the epoxidation of cyclohexene [45]. However, it wasn't until 2011 that the term "single-atom catalyst" was formally introduced. Zhang et al. were the first to conceptualize SACs, synthesizing a highly efficient Pt/FeOx catalyst that demonstrated remarkable selectivity in the oxidation of carbon monoxide. They also employed DFT calculations to show how the platinum sites were stabilized on the support and elucidated the mechanism behind the selective oxidation of carbon monoxide [46]. There are various synthesis pathways for producing SACs, which can generally be divided into dry chemistry and wet chemistry routes [47]. Dry chemistry methods include techniques such as atomic layer deposition, ball-milling, two-step doping, and pyrolysis. The pyrolysis method involves decomposing an organic precursor at elevated temperatures in a controlled atmosphere. This approach is particularly effective for transition metals, with the choice of support material depending on its ability to

withstand high temperatures. The interaction between the metal and the support is crucial for maintaining atomic dispersion following heat treatment.

In contrast, the wet chemistry routes for synthesizing SACs are more varied. Numerous methods have been proposed in the literature, including photoreduction, galvanic replacement, ion-exchange, and wetness impregnation methods. The wetness impregnation method is a common approach for preparing heterogeneous catalysts, wherein an aqueous or organic metal salt is impregnated onto the catalyst support. The excess solvent is then removed by evaporation. This method heavily relies support surface area, which should provide adequate anchoring sites for the metal atoms. Furthermore, the interaction between support and metal is vital, as it influences the metal loading and helps prevent aggregation. SACs possess unique structural characteristics that enable them to demonstrate higher specific activity, stability, and selectivity compared to nanoparticle catalysts. They can achieve atomic utilization efficiencies of nearly 100%, meaning that every metal atom is in contact with the reactants. Despite their promising advantages, SACs do have limitations. One major drawback is the absence of ensemble sites adjacent to the single atom, making them less suitable for surface reactions involving larger molecules. For instance, their selectivity in C-C coupling reactions is restricted, and in carbon dioxide reduction reactions (CO₂RR), the products are typically limited to C1 species due to the lack of neighboring atoms. [48, 49]. Additionally, to avoid aggregation, the metal loading in SACs must be kept low, which can lead to reduced overall activity compared to nanoparticle catalysts.

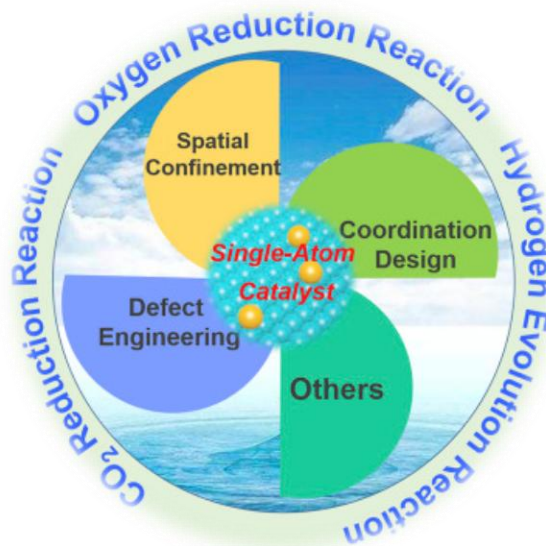


Figure 1. 7 SAC Applications Overview [50]

1.7.2. Dual Atom Catalyst

Dual-atom catalysts (DACs) consist of pairs of metal atoms evenly spread across a support material. They build on the concept of single-atom catalysts (SACs) and can help address some of the challenges faced by SACs. The interaction between the two metal atoms can modify the electronic properties of the active sites, enhancing the catalyst's performance. Unlike SACs, DACs often excel in complex reactions involving larger molecules. They are particularly effective for carbon-carbon (C-C) coupling and can help produce C₂ compounds such as ethylene (C₂H₄) or ethanol (C₂H₅OH) in carbon dioxide reduction reactions (CO₂RR) [51]. Dual-atom catalysts (DACs) can be categorized into two types based on whether the metal pairs are the same or different:

- I. Homonuclear DASC
- II. Heteronuclear DASC

Homonuclear DACs are made up of two identical metal atoms that are positioned next to each other on a substrate. These atoms may have the same or different oxidation states. The interaction between these two metal sites can enhance certain reactions by creating additional active sites for attaching reactants or intermediates during the catalytic

process [48]. Heteronuclear dual-atom catalysts consist of two distinct metal atoms, allowing for a wide range of combinations. The interactions and synergistic effects between these different metal atoms can lead to unique electronic structures, potentially resulting in enhanced performance compared to homonuclear dual-atom catalysts. Advances in theoretical methods, such as density functional theory calculations, machine learning, and molecular simulations, play a crucial role in the design of these catalysts. This is especially important given the challenges associated with synthesizing well-dispersed heteronuclear catalysts and the numerous combinations of metal atoms available [52].

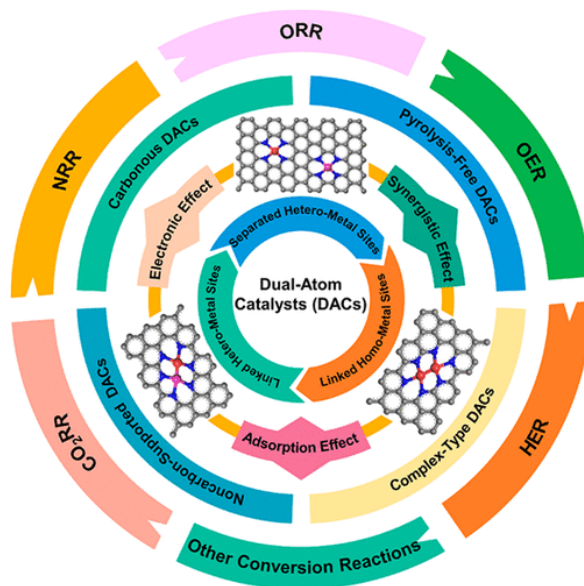


Figure 1. 8 DAC Types and Applications Overview [49]

SAC showed impressive performance in single-molecule elementary reactions, such as HER and ORR. However, their inherent simplicity has hindered their effectiveness in multi-step reactions. For example, in electrocatalytic processes like the electrochemical reduction of CO₂ (CO₂RR), SACs often fall short compared to other catalysts. In contrast, dual-atom catalysts (DACs) present numerous opportunities to broaden the scope of electrocatalysis. These catalysts can address the complexities of various reactions by combining the benefits of SACs with a greater variety of functionalized sites. For instance, DACs have been predicted to facilitate the production of C₂ products in CO₂RR, whereas SACs are typically restricted to generating only C₁ products.

The reaction mechanism for carbon dioxide reduction (CO₂RR) using dual-atom catalysts (DACs) has been predicted through DFT calculations [51]. The main difference between SAC and DAC carbon-carbon (C-C) coupling, which is enhanced by the larger size of the metal pairs. This enhancement occurs due to various intermediates absorbing onto the metal pairs, leading to the formation of C₂ products (C₂H₄, C₂H₅OH).

It has been found that co-adsorbed carbon monoxide (CO) molecules act as intermediates that facilitate C-C coupling. These CO molecules can dimerize to form OCCO dimers, which help generate C₂ products. The specific ways CO molecules are absorbed play a major role in this dimerization process, further enhanced by metal pairs in DACs. Unlike SACs, there have been successful reports of producing ethylene using heteronuclear dual-atom catalysts

Currently, dual-atom catalysts (DACs) are gaining popularity in electrocatalytic reactions and have also demonstrated impressive performance in various organic reactions. For instance, copper-dimer catalysts exhibit high selectivity in the partial oxidation of methane, achieving a 10% photocatalytic conversion of methane (CH₄) with O₂, specifically targeting methyl oxygenates [53]. This enhanced selectivity is attributed to the presence of Di copper-oxo centers, which effectively catalyze the partial oxidation of methane. In contrast, copper monomers only facilitate methane oxidation, resulting in lower selectivity.

1.8 Problem Statement

Primary challenges facing zinc-air batteries (ZABs) is development of stable & efficient dual function electrocatalyst oxygen electrode, which can effectively address the sluggish reaction kinetics associated with both ORR & OER. These reactions are crucial for the overall performance of ZABs. However, the sluggish kinetics of these reactions often lead to high overpotentials, reducing the overall energy efficiency of the system. Despite significant advancements, achieving a bifunctional catalyst that can perform both reactions with high efficiency and stability remains a significant challenge. This is mainly due to the differing reaction mechanisms and required catalytic properties

for ORR and OER, which makes it difficult to design a single material that can perform both reactions effectively. In addition, stability of these electrocatalysts under the operating conditions of ZABs for longer time is another major hurdle. The air electrode experiences fluctuating conditions, including varying current densities and potential cycling, which can lead to catalyst degradation over time. This degradation results from processes such as corrosion, oxidation, and the dissolution of active sites, ultimately reducing the catalyst's performance and lifespan.

1.9 Research Objectives

The primary aim of this study is

- Develop a durable, efficient, and cost-effective bifunctional electrode for zinc-air batteries
- Investigate catalyst properties affecting ORR and OER activities
- Synthesize and optimize CoMn-N-C/N-MC bifunctional electrocatalysts
- Analyze structure and morphology using SEM, XRD, etc.
- Correlate structural features with electrocatalytic performance
- Evaluate activity, stability, and efficiency under operational conditions

CHAPTER 2: LITERATURE REVIEW

Manh-Kien Tran et al discusses the role of different kinds of zinc-air batteries for electric vehicles. The potential and suitability of primary and secondary batteries is summarized for electric vehicles where high energy & power density is required. For chemical recharging, fast recharging and stable battery chemistry must be ensured. The charging and discharging are driven by OER & ORR. A high performance dual functional electrocatalyst has prime importance in such batteries [54].

ZIFs have remarkable qualities that make them very promising for wider application, particularly in the field of catalysis. These properties include excellent chemical stability obtained from metal-N bonds, specific surface area and pore size [55],[56]. Important methods of converting chemical processes into energy include electrocatalysis, photocatalysis, and organic catalysis. Consequently, it's critical to create catalysts with superior stability and activity. When properly heated and/or chemically treated, the ZIF hybrid materials formed by using the template approach increase the efficiency of catalytic reactions [57]. A high active specific surface area porous structure efficiently facilitates the transport of ions or molecules.

Building well-defined structures with more tri-phase interphases can also greatly benefit from hollow architecture with its large specific surface area and well-defined void space. Fe-doped Co/Co₃O₄ with a mesopore-rich concave surface that was encased in hollow carbon was formed by pyrolysis of MOF precursors with the help of a NaCl template [58]. The catalyst's special structure made it easier for oxygen molecules to collide with one another on its inner and outer surfaces and to use its active sites to their fullest potential. Synthesized material when addition of Fe element showed good ORR & OER performance. The Zn-air batteries made with the designed electrocatalysts demonstrated exceptional durability over an extended period and excellent charge-discharge cycle capability.

KCl particles and ZIF-67 were used in the salt-template process to create single Co-N sites. The resultant monodispersed, had a very high Co loading of approximately 17.3

weight percent and as KCl encapsulation prevents ZIF-67 layer from shrinking during pyrolysis with high temperature, KCl played a critical role in the salt-template method. Consequently, the immobilization of the Co atoms in the ZIF leads to a limited size of 0.10–0.40 nm and reduces the aggregation of Co particles. The Co-N sites of SCoNC, which were densely populated, demonstrated a good bifunctional catalytic activity, for OER it showed at 10 mA cm^{-2} at 1.54 V, 74 mV dec^{-1} Tafel slope and for ORR process it showed half-wave potential ($E_{1/2}$) of 0.91 V [59].

In another work, Co@N-CNTs/3DHC electrocatalyst was designed. A NaCl-template technique that includes the following steps: carbonization, freeze-drying, and finally removing the template; was used to fabricate a 3DHC (3D honeycomb carbon) substrate with honeycomb-like nano-chambers. Encouraging the uniform growth of BZIFs nanocrystals using the confinement principle, these nano-chamber structures can serve as suitable nanoreactors. Co@N-CNT assembly, in which cobalt nanoparticles are encased by N-CNT shells that obtained by meticulously pyrolyzing the confined BZIFs nanocrystals [60].

Among different carbon templates/substrates CNTs are also famous one because e^- of the C atom on CNTs develop off-domain π -bonds of large range, which have a big impact on conjugation [61]. Figure 2.1 (a), by pyrolyzing ZIF grown on oxidized carbon nanotubes (OCNTs), Sheng et al. Synthesized carbon fragments that rich in atomically dispersed metal nitrogen carbon sites. The $E_{1/2}$ is 0.865 V and OER overpotential of 0.442 V at 10 mA cm^{-2} , which is lower than combination without CNTs. This catalyst based RZABs gives 182 mW cm^{-2} power density of 1000 h at 10 mA cm^{-2} cyclic stability, better than commercial Pt/C & other reported catalyst. Figure 2.1 b-d depicts morphology of the Fe-ZIF/OCNT products manufactured under optimal conditions. Figure 2.1 e depicts the energy dispersive X-ray ESEM, which reveals a similar or homogenous distribution of N, C & Fe. HAADF-STEM pictures (Figure 2.1 f-g) considerable number of solitary bright spots caused by iron or residual zinc atoms are evenly dispersed over the carbon sheet. The abundance of controlled active sites, the combination of several effective single-site catalysts, and the CNT network's good charge/mass transfer dramatically increased ORR & OER performance [62].

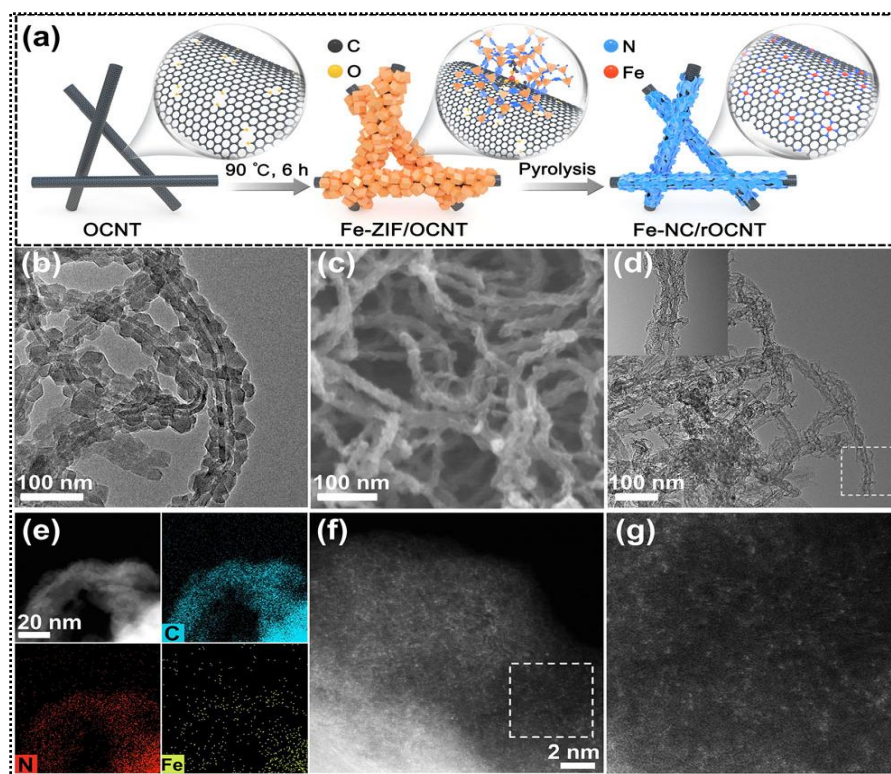


Figure 2. 1 a) Schematic illustration for the synthesis of Fe-NC/rOCNT hybrids. b) TEM image of Fe-ZIF/OCNT. c) SEM image. d) TEM image of Fe-NC/rOCNT. e) EDS mapping of Fe-NC/rOCNT. f) HAADF-STEM image of Fe-NC/rOCN

Kalsoom Zahra et al summarize and comment on the various strategies adopted to develop electrocatalysts based on cheap transition metals. The advantages and disadvantages of strategies are discussed important contributions are highlighted. The transition metal based electrocatalysts are very potent candidates for oxygen reactions in rechargeable metal air batteries, fuel cells and electrolyzes [63].

Jiarun Cheng et al study the effect of phosphorus and sulfur doping on ORR selectivity of nitrogen doped carbon spheres. The electronic structure of N-doped carbon was modified because of dopants and facilitated the ORR by two-electron route. The mechanisms of observed results are investigated in detail, and it is concluded that the graphitic-N is mainly responsible for improving the kinetics of ORR. The presence of heteroatoms allows control over materials properties by adjusting their doping ratio [64].

Lianhui Wu et al discuss the influence of surface reconstruction on oxygen evolution reactions and methods to control the extent of surface reconstruction for transition metal-based catalyst. The prepared catalyst acts as a pre-catalyst that undergoes surface reconstruction during which its activity is increased. In this way the actual catalyst is obtained that catalyzes the OER. It is important to adopt suitable strategies to achieve controlled and optimized surface reconstruction. Such strategies include doping, leaching and particle size regulation are discussed [65].

Fang Dong et al discuss recent progress and future directions of metal-nitrogen-carbon (M-N-C) materials. These materials are based on abundant transition metals and cheap elements, i.e., nitrogen and carbon. They have great potential to replace Pt based electrocatalyst for ORR due to high activity, efficient utilization of loaded metal and low cost. However, the current synthesis methods are still expensive and not suitable for commercial purposes. Methods to design the M-N-Cs and prominent strategies for improving the bifunctional performance are highlighted [66].

He Sun et al reports on a strategy to improve the intrinsic activity of single atom active sites that will consequently improve the energy efficiency of the reaction. For this purpose, a P-O bond is introduced in the catalyst system that alters and adjusts the electronic structure of the catalyst. The concept is also evaluated by using density functional theory and it is observed that P-O bond is responsible for enhanced bifunctional properties. An excellent half wave potential of 0.89 V is obtained against reversible hydrogen electrode (RHE). The reported materials performed impressively for aqueous as well as solid state zinc air batteries [67].

Licheng Wei et al discuss various types of modifications of transition metal based electrocatalysts that can potentially be employed in commercial zinc-air batteries. The modifications include formation of nitride, oxides, or phosphides of the metals. It is also important to tune the conductive properties of support material. The significance of single atom catalysts based on transition metals is highlighted and the strategy of rationally combining different metals is also discussed [68].

Jing Wang et al studied the effect of incorporation of axial oxygen in M-N-C based catalysts for the catalyzing the electrochemical reduction of carbon dioxide. It is observed that the number of electrons in d-shell of outermost orbital and electronegativity of elements has great effect on the materials properties and catalytic activity. This strategy helped to significantly improve the intrinsic activity and stability of the prepared catalysts. M-N-Cs based on different metals (for example Mn, Cr, Os, Ru and Rh) were studied by using volcano plots [69].

Eric Musa et al used machine learning to explore the properties of single atom catalysts. The methods to select the appropriate catalyst for are discussed for various reactions like OER, ORR and HER. The methods to use machine learning for rationally designing catalysts are also summarized [70].

Wenzheng Cheng et al studied the contribution of topological defects in improving the activity of Fe-N₄ based active sites. Defective carbon nanosheets doped with nitrogen and phosphorus showed excellent results for both OER and ORR. A half wave potential of 0.903 V was obtained. The catalyst was tested in zinc air batteries and a good cycle life was observed [71].

2.1 Research gap

Despite significant progress in the development of bifunctional electrocatalysts for zinc-air batteries (ZABs), several research gaps remain. One of the primary challenges is the limited performance of existing bifunctional catalysts. Many current catalysts struggle to achieve high efficiency for both the oxygen reduction reaction (ORR) and oxygen evolution reaction (OER), often exhibiting a trade-off between the two. Identifying new materials or innovative combinations of metals that can deliver optimal performance for both reactions is essential. Additionally, while some catalysts show promising activity, they often lack long-term stability. Under the harsh operating conditions of ZABs, such as fluctuating current densities, high potentials, and cycling, catalysts can degrade due to corrosion, oxidation, or the loss of active sites. This instability severely impacts their practical application. Further research is needed to address the durability of these materials and enhance their performance over extended periods.

2.2 Purposed Solutions

To address these challenges, one potential solution is the design of new bifunctional catalysts with optimized performance for both ORR and OER. This could involve exploring new metal combinations, dual-metal systems, or atomic-level precision in catalyst design to enhance catalytic activity for both reactions. Improving the stability of catalysts can be achieved through material engineering along with this scalability and cost-effectiveness of synthesis methods must be addressed. Developing low-cost precursors and green synthesis routes, along with scalable deposition techniques like atomic layer deposition (ALD) or electrochemical deposition, could make advanced catalysts more accessible for commercial use. These solutions could help bridge the existing gaps and lead to the development of more efficient, durable, and scalable bifunctional electrocatalysts for ZABs, contributing to the advancement of sustainable energy storage technologies.

CHAPTER 3: INTRODUCTION TO EXPERIMENTAL TECHNIQUES

3.1 Physical Characterizations

Since it provides details about the material's shape, composition, and crystallite size, X-ray diffraction, or XRD, is a crucial tool for material characterization. To complete the process, the X-ray radiation must be sent through the material at an angle. The measurement of the diffraction angle and intensity, which yields details about the structural morphology of the material under investigation, is the next step. The patterns of X-ray diffraction (XRD) in crystalline materials are predicated on the fact that X-rays can exhibit two distinct behaviors: waves and particles.

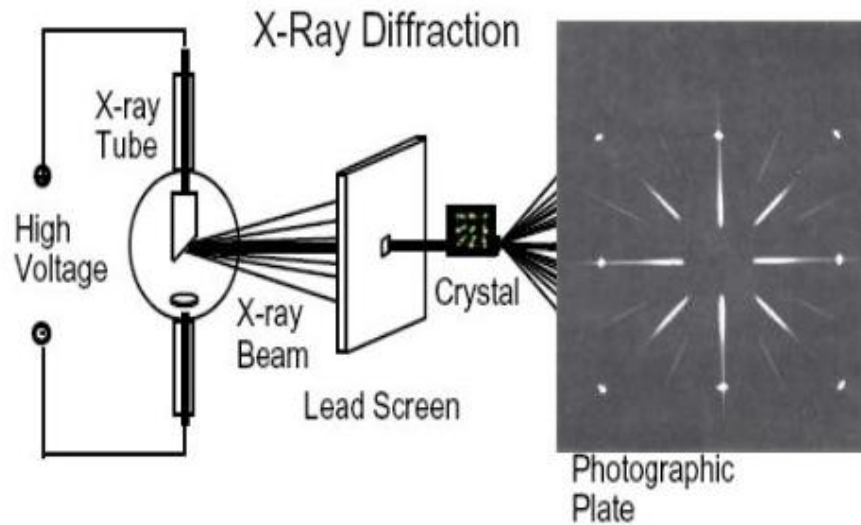


Figure 3. 1 A schematic of X ray diffraction

The fundamental purpose of this technique that is employed is to identify and characterize materials based on the X-ray diffraction patterns of such materials. They make use of this technology. Diffraction is the term for the phenomena that occurs when a monochromatic X-ray beam strikes a substance. The Law of Bragg governs this phenomenon. Interference, which can be constructive or destructive, is a characteristic of

crystalline structures. The atoms that make up the material are the source of this disturbance.

$$2d \sin(\theta) = n(\lambda) \quad (3.1)$$

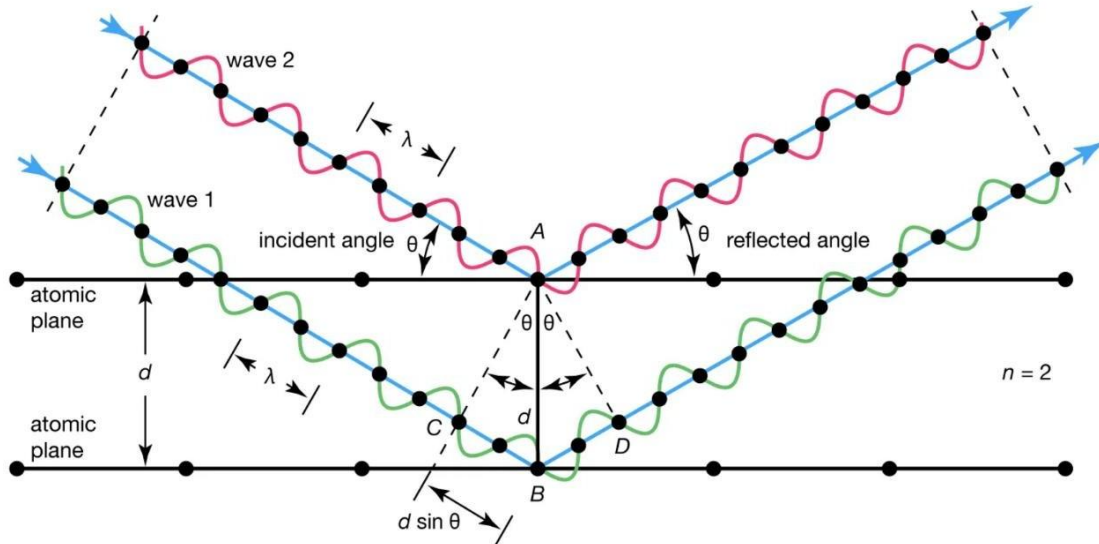


Figure 3. 2 The Bragg's Law [11]

The accessible directions of diffraction are determined by the size and shape of the unit cell in the material, and the intensity of the diffracted waves is influenced by the arrangement of atoms within the crystal lattice. Numerous small crystallites grouped in various orientations make up many materials. These crystallites are known as aggregate or polycrystalline powder. Anytime an X-ray beam strikes a material, it interacts with every available interatomic plane. By changing the experimental angle, this interaction enables the identification of every diffraction peak.

A high-energy electron beam is used in SEM to produce a range of signals on an object's solid surface. These electrons can move through the material and come out on the other side, as shown in Figure 3.3. The material's crystalline structure, surface appearance, material orientation, and chemical makeup can all be inferred from the interactions that occur between the electron beam and the sample.

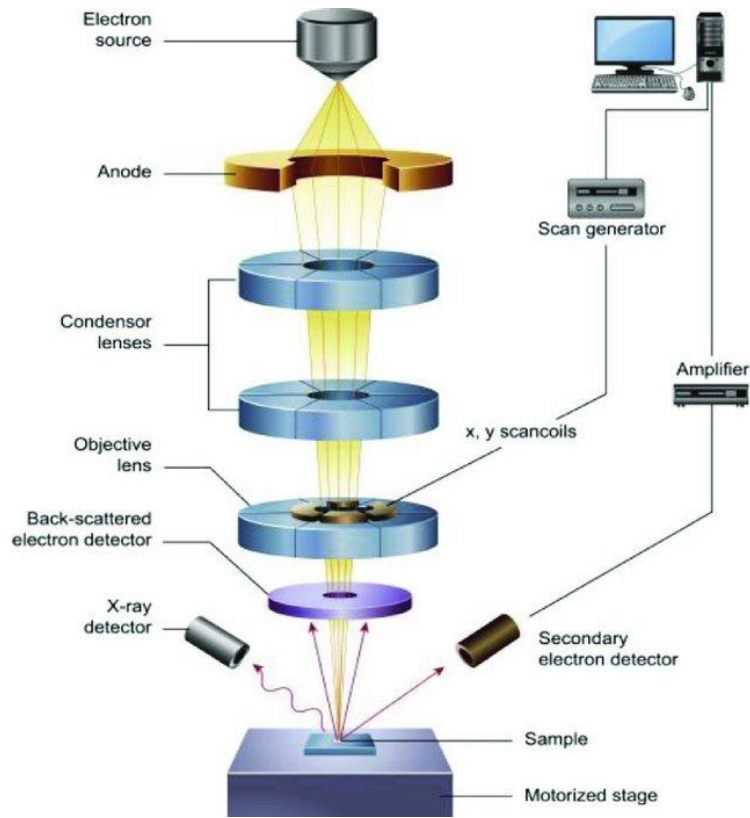


Figure 3. 3 Illustration of how SEM works [72]

Usually, the SEM produces two-dimensional images that show spatial variations in the material's surface characteristics. The basic scanning electron microscope (SEM) technology may use magnification (20X to 30,000 X) and a three-dimensional resolution of 50 to 100 nm to differentiate between areas that are between 1 cm and 5 microns in size. This method is particularly useful for analyzing crystalline structures, determining crystal orientations (EBSD), and performing semi-quantitative or qualitative studies of chemical components (EDS). This scanning electron microscope (SEM) is like EPMA in terms of both design and function, and it can do specialized area or point location examinations on samples.

TEM is a high-resolution imaging tool used to analyze materials at the nanoscale. Using this technique, a sample is exposed to an electron beam, and the interaction between the electrons and the sample is used to create a graphic representation on the screen. Transmission electron microscopy (TEM) uses electromagnetic lenses to concentrate a

high-energy electron beam from an electron gun onto a thin sample. The density and thickness of the sample determine how the electrons behave when they encounter the material, whether they are transmitted, absorbed, or scattered. By revealing the inner structure of materials at the atomic level, TEM facilitates the investigation of flaws and dislocations that are challenging to detect using conventional methods. Instrumentation TEM is divided into four sections:

- i. Electron Gun
- ii. The system of EM lenses
- iii. Mount
- iv. Visual apparatus

The surface analysis technique XPS, used to identify oxidation state. Surface of sample is bombarded with rays of X-rays, which causes the atoms there to release electrons known as photoelectrons. This is what allows the instrument to work.

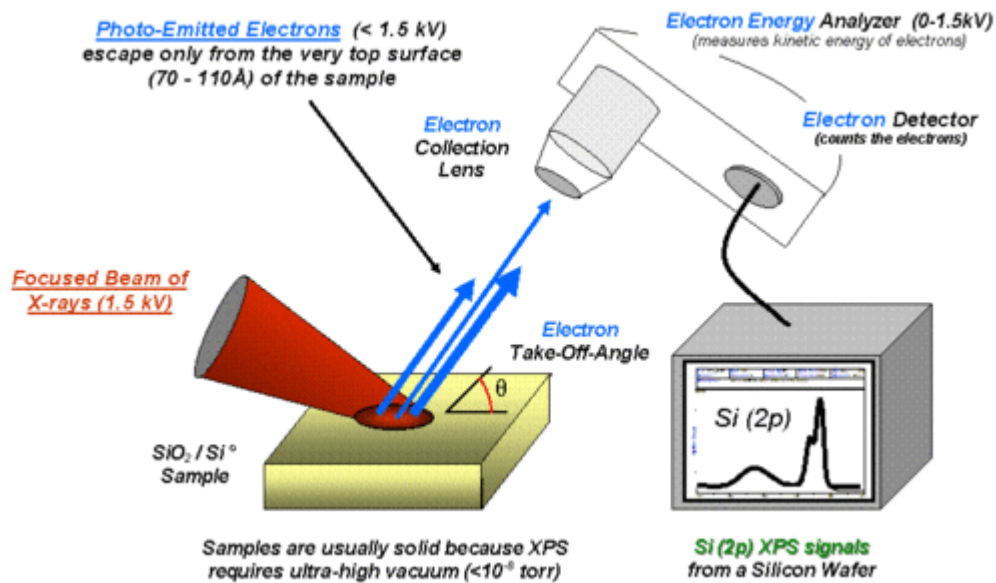


Figure 3. 4 Working principle of XPS [5]

These photoelectrons' properties are then ascertained by analyzing their kinetic energy and emission angles. Usually, the X-ray beam's energy is set to be higher than the

electrons' binding energy in the sample's valence band. By means of absorption, X-ray photons possess the ability to create a positively charged ion by removing one electron from the valence band. Atom electronic structure, including its chemical composition and bond state, can be determined by measuring the kinetic energy of these emitted photoelectrons using an electron analyzer.

3.2 Electrochemical Characterization

The electrochemical properties of the materials and their applicability for charge-discharge functions in zinc-air batteries were evaluated using important technique:

- Cyclic Voltammetry (CV)
- Linear sweep Voltammetry (LSV)
- Electrochemical Impedance Spectroscopy (EIS)

A widely used technique known as CV is used for the analysis of electrochemical reactions and their kinetics. Generally, CV studies provide insights into electroactive material's redox behavior [73, 74]. During analysis of CV, voltage of stationary working electrode in a non-stirred solution is change. [74].

From the Curves of CV, we can determine desorption and adsorption of oxygen species on surface of catalyst, indicated by the presence of specific peaks in the lower voltage region [75, 76]. Similarly, redox behavior of oxygen can be observed through corresponding peaks in the higher voltage regions during the forward and reverse scans [77, 78]. The CV profile offers essential information about the electrocatalysts.

LSV specialized technique used for the study of redox behavior of species that it electroactive species by applying voltage in both anodic (reverse, moving from upper limit to lower limit) and cathodic sweeps [79]. Unlike cyclic voltammetry (CV), LSV records data in only one direction, either forward or backward.

When LSV is conducted under hydrodynamic conditions, it helps us understand electron transfer rate between the electrode and the electrolyte. This information is valuable for evaluating mass transfer effect and kinetics involved in reaction [80, 81].

The kinetics of the ORR can be evaluated through factors such as current density, specific activities obtained from curves of LSV[82]. By examining LSV profiles under specific conditions, we can gain a clear understanding of the electrocatalytic performance of the materials.

EIS technique is used to study the electron transfer processes occurring at the interface of electrode electrolyte during reactions [83]. It is a valuable method for gaining insights into chemical transformation involved in these reactions.[84]. For investigation of intrinsic properties of catalyst material EIS is commonly employed as intrinsic property impact efficiency and conductivity of fuel cell [85]. EIS is typically characterized by following factors:

- i **Ohmic Resistance**
- ii **Double-Layer Capacitance**
- iii **Charge Transfer Resistance**

Additionally, the diffusion properties of electroactive species, resulting from the adsorption of reactants or products on surface of electrode, is Warburg impedance [84]. Depending on the materials being studied and the type of information required for accurate evaluation. Figure 3.5. A typical EIS (Nyquist plot) diagram illustrating an electrical circuit fit. The plot features complex Cartesian coordinates, with the real axis representing the resistive component and the imaginary axis representing the capacitive or impedance component [84].

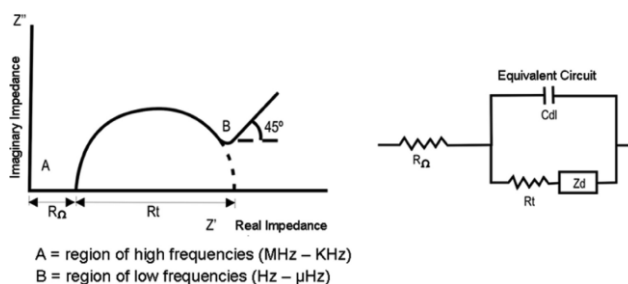


Figure 3. 5 Nyquist plot and its corresponding equivalent circuit, illustrating the influence of diffusive impedance [84]

CHAPTER 4: METHODOLOGY

4.1 Material Collection and Methods

4.1.1 Material Collection

For preparation of Co Mn-N-C/N-MC electrocatalyst all reagents & chemicals were high analytical grade, and these materials sourced from sigma-Aldrich and utilized directly without any further processing. The chemical and reagents employed in synthesis includes Ni (NO₃)₂·6H₂O (nickel nitrate hexahydrate), Mn (NO₃)₂·6 H₂O (manganese nitrate hexahydrate), Co (NO₃)₂·6 H₂O (cobalt nitrate hexahydrate), 2-methylimidazole, 1-10 Phenanthroline monohydrate, Hydrophilic nano silica (15nm), methanol, DI water and HF.

4.1.2 Synthesis of Mn-N-C/N-MC

Mn(CH₃COO)₂·4H₂O was used as the metal precursor for the synthesis of Mn-N-C/N-MC, following a modified procedure based on reported literature [86]. Initially 1,10-phenanthroline monohydrate (0.094 g) was dissolved in 20 mL methanol and stirred for 25 mints. Then, 2-methylimidazole (0.66g) was added. The mixture was stirred for another 55 mint and then added into Hydrophilic nano silica (1 g) under stirring after 6 to 7 hours of stirring gel-like structure formed and Methanol evaporated at 75 °C. The collected sample was pyrolyzed in a tube furnace at 800 °C for 3 h under flowing argon. The obtained sample was denoted as Co Mn-N-C/OMC. HF solution is used to remove silica template. The obtained sample was denoted as Mn-N-C/N-OMC.

4.1.3 Synthesis of Co-N-C/N-MC

Here Co (NO₃)₂·6 H₂O were used as the metal precursors. Initially 1,10-phenanthroline monohydrate (0.094 g) was dissolved in 20 mL methanol and stirred for 25 mints. Then, 2-methylimidazole (0.66g) was added. The mixture was stirred for another 55 mint and then added into Hydrophilic nano silica (1 g) under stirring after 6 to 7 hours of

stirring gel-like structure formed and Methanol evaporated at 75 °C. The collected sample was pyrolyzed in a tube furnace at 800 °C for 3 h under flowing argon. The obtained sample was denoted as Co-N-C/OMC. HF solution is used to remove silica template. The obtained sample was denoted as Co Mn-N-C/N-OMC.

4.1.4 Synthesis of Co Mn-N-C/N-MC

Co (NO₃)₂·6 H₂O and Mn (CH₃COO)₂·4H₂O were used as the metal precursors in a 1:1 molar ratio, respectively. Initially 0.094 g of 1,10-phenanthroline monohydrate was dissolved in 20 mL of methanol and mixed for 25 minutes. Afterwards 0.66 g of 2 methylimidazole was added to the solution. This mixture was agitated for an additional 55 minutes and then added in Hydrophilic nano silica (1 g) under stirring after 6 to 7 hours of stirring gel-like structure formed and Methanol evaporated at 75 °C. The Collected sample subjected to pyrolysis in tube furnace at a temperature of 800°C for a duration of 3 hours with an argon gas flow maintained thorough out process. HF solution is used to remove silica template. The obtained sample was denoted as Co Mn-N-C/N-M. The Synthetic Process of catalyst is shown in Figure 4.1

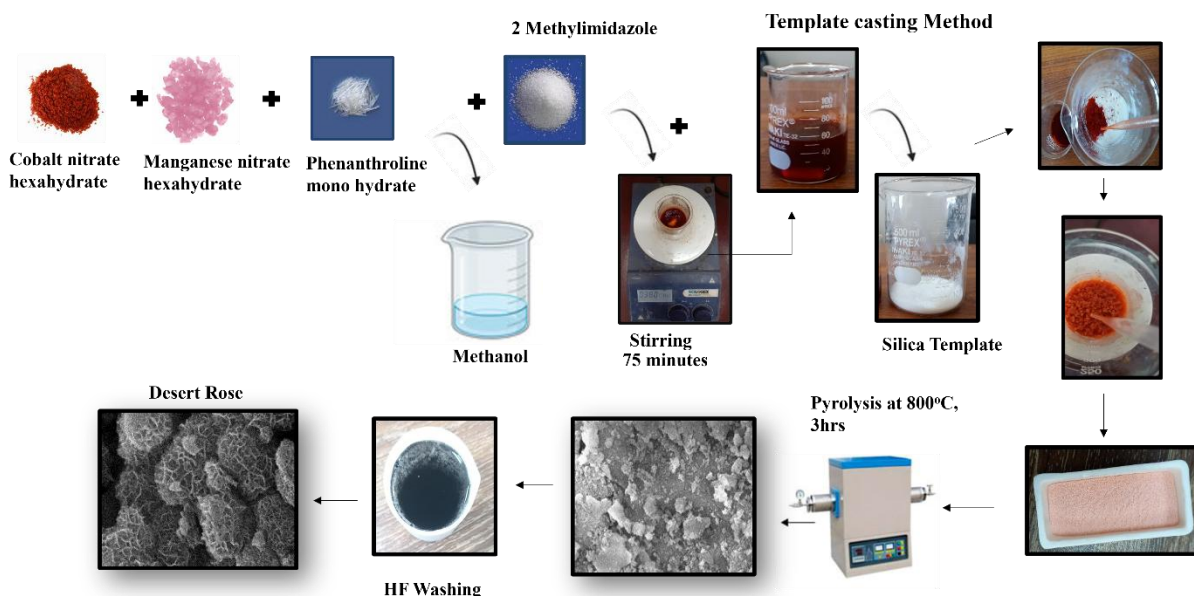


Figure 4. 1 Schematic representation of Co Mn-N-C/MC

CHAPTER 5: RESULTS AND DISCUSSION

5.1 X-Ray Diffraction (XRD)

The crystalline structure of the synthesized CoMn-N-C/N-OMC material was examined using X-ray diffraction (XRD). The XRD pattern of the mesoporous carbon structure, pyrolyzed at 800°C, is presented in Fig 5.1. The material exhibited two distinct diffraction peaks at approximately 25° and 43°, which correspond to the (002) and (101) planes of graphitic carbon, respectively. These reflections indicate the formation of N-doped graphitic carbon, suggesting the presence of a conductive, amorphous carbon framework. Interestingly, the XRD pattern showed no prominent peaks corresponding to metal or metal oxide phases, such as Co or Mn-based oxides. This absence suggests that the Co and Mn atoms were successfully embedded as atomically dispersed species within the carbon matrix rather than forming separate metal clusters or oxide particles. The lack of metal or oxide peaks is further indicative of a homogeneous distribution of dual Co and Mn atoms within the carbon framework, which is advantageous for electrocatalytic applications by providing highly accessible and active atomic sites. The absence of Co and Mn clusters is consistent with the small amounts of these metals introduced during synthesis, confirming that only trace amounts of the metals are integrated into the carbon structure. This result demonstrates the effectiveness of the template-casting method in producing atomically dispersed dual-metal catalysts without agglomeration, a key feature for achieving high catalytic performance [87].

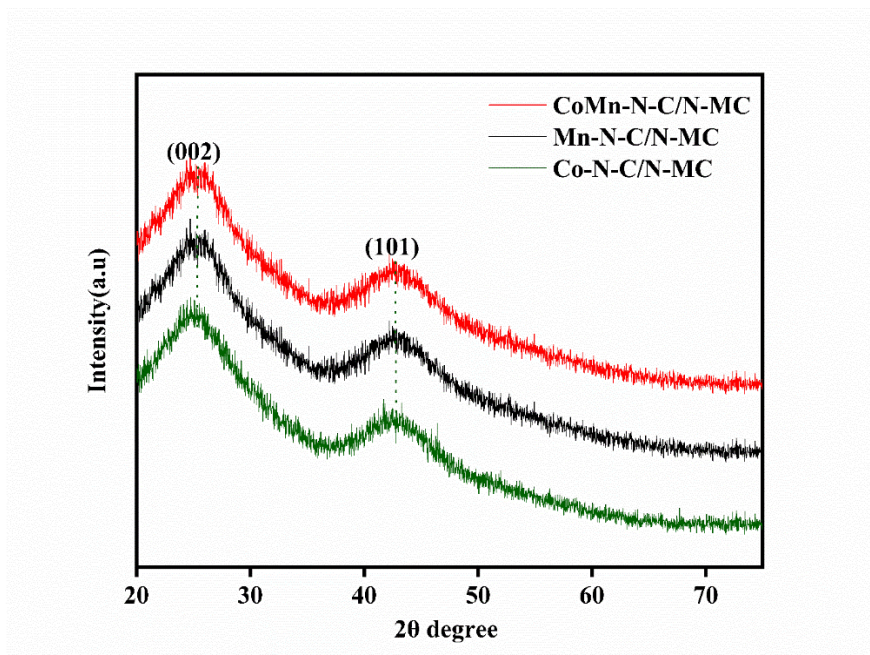


Figure 5. 1 XRD pattern of Co-N-C/N-MC, Mn-N-C/N-MC Co Mn-N-C/N-MC

5.2 Scanning Electron Microscopy

The Scanning Electron Microscopy (SEM) analysis of the CoMn-N-C/N-MC catalyst provides valuable insight into the evolution of its morphology before and after acid washing. In the SEM micrograph shown in Figure 5.2 (a), the sample displays a porous structure, but the pores are not clearly visible, likely due to the presence of residual silica from the template used during the synthesis. This incomplete removal of the silica template during the pyrolysis process obscures the finer details of the pore network, resulting in an irregular structure. However, after the sample undergoes acid washing with hydrofluoric acid (HF) to remove the silica template, the morphological changes are striking, as shown in Figure 5.2 (b). The acid-washed sample reveals a well-organized 3-dimensional open framework with a desert rose-like structure, characterized by petal-like formations and interconnected layers, providing a high degree of mesoporosity. The successful removal of the template not only exposes the mesoporous channels but also ensures that the structural integrity of the carbon framework is preserved. This porous structure offers enhanced surface area, facilitating the rapid transport of ions and reactants through the interconnected pores. Such a highly accessible and interconnected framework makes the CoMn-N-C/N-

MC catalyst ideal bifunctional electrocatalyst, where efficient mass and charge transfer are critical for performance. The transformation from an unclear porous structure to a well-defined, open mesoporous framework highlights the effectiveness of the synthesis and acid-washing processes in creating a material with improved functionality and catalytic potential.

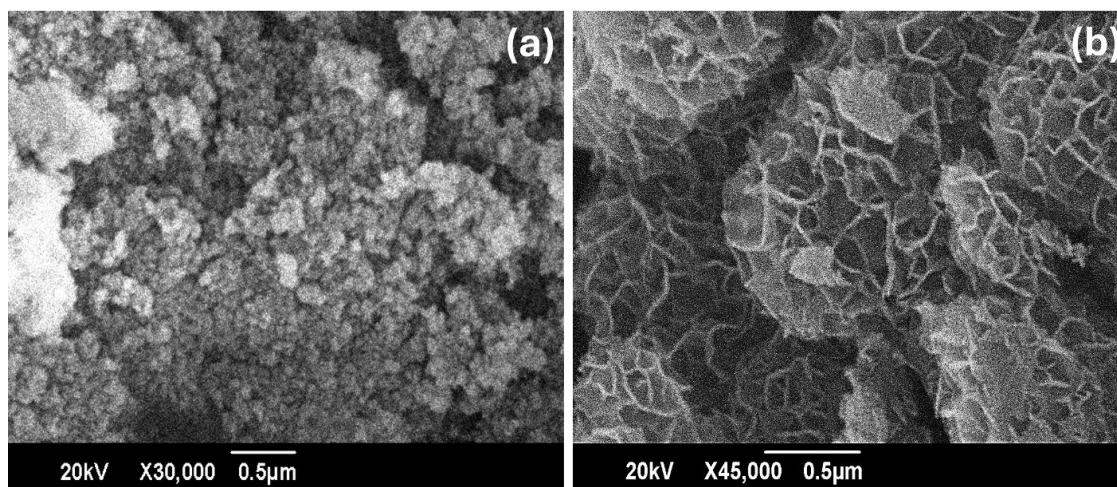


Figure 5. 2 SEM images of Co Mn-N-C/MC (a) After pyrolysis (b) After acid etching

5.3 Brunauer-Emmet-Teller (BET) Analysis

To analyze the surface area and pore size of the synthesized CoMn-N-C/N-OMC catalyst, nitrogen adsorption-desorption (N_2 sorption) measurements were performed. The nitrogen sorption isotherms, presented in Figure 5.3 (a), exhibit a type-IV adsorption-desorption profile, which is characteristic of mesoporous materials. This type of isotherm indicates the presence of well-developed mesopores, with a distinct hysteresis loop associated with capillary condensation within the mesoporous structure. The Barrett-Joyner-Halenda (BJH) analysis reveals that the average pore size of the CoMn-N-C/N-OMC framework is approximately 3.6 nm, as shown in Figure 5.4 (b), confirming the successful formation of mesopores. Additionally, the specific surface area of the catalyst is measured to be $136 \text{ m}^2 \text{ g}^{-1}$, while the pore volume is determined to be $0.94 \text{ cm}^3 \text{ g}^{-1}$, both of which are indicative of a highly porous structure. The combination of a high surface area and a well-defined pore network ensures that the catalyst offers abundant active sites and enhanced accessibility for reactants, making it highly suitable for applications such as

catalysis and energy storage. This mesoporosity, combined with atomic-level dispersion of Co and Mn, enhances mass transport and ensures efficient utilization of active sites, contributing to the material's excellent performance potential.

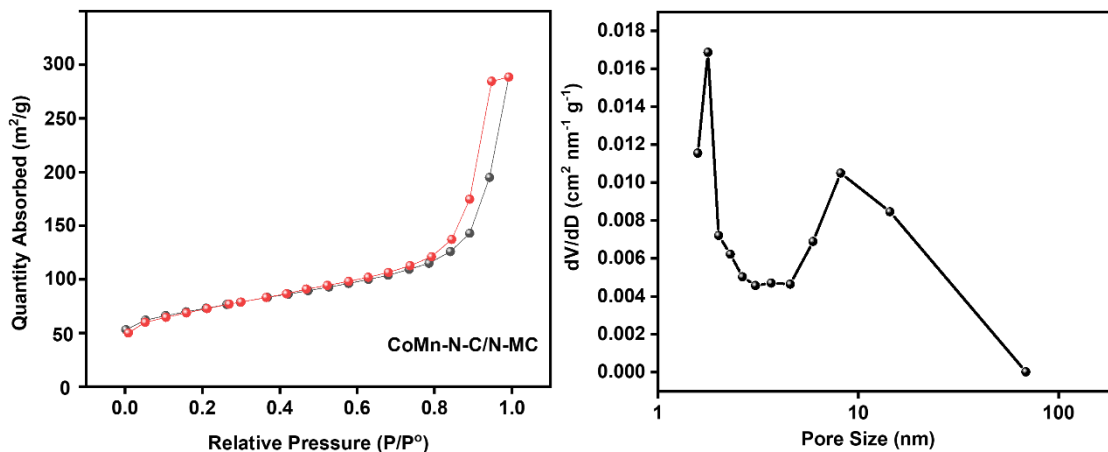


Figure 5. 3 BET analysis (a) N_2 -sorption isotherms of CoMn-N-C/N-MC, (b) pore size distribution CoMn-N-C/N-MC

5.4 Raman Spectroscopy

The Raman spectrum of the CoMn-N-C/N-MC, Co-N-C/N-MC and Mn-N-C/N-MC catalyst presented in Figure 5.4. Spectrum provides further insights into the structural characteristics of the N-doped mesoporous carbon framework. The spectrum exhibits two prominent peaks: the D-band at 1349 cm^{-1} and the G-band at 1579 cm^{-1} . The D-band is associated with the defects and disorder in the carbon structure, while the G-band corresponds to the in-plane vibrations of sp^2 -hybridized carbon atoms in graphitic domains. Here CoMn-N-C/N-MC, Co-N-C/N-MC and Mn-N-C/N-MC showed intensity ratio of 1.07, 0.93 and 0.92. The intensity ratio I_D/I_G of 1.07 suggests a moderate degree of structural disorder, which is typical for N-doped carbon materials. The presence of both D and G bands, along with their nearly equal intensity, reflects a balance between defects introduced by nitrogen doping and the retained graphitic features of the carbon framework. This balance is crucial as the defects increase the number of active sites for catalysis, while the graphitic domains enhance the electrical conductivity of the material. The Raman analysis,

therefore, confirms that the CoMn-N-C/N-MC framework exhibits a partially graphitized structure with sufficient defects.

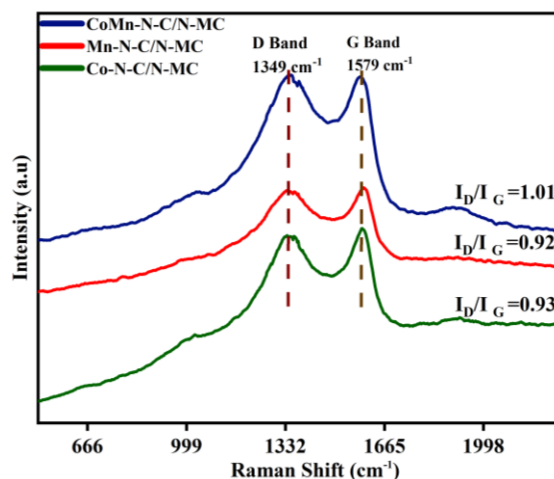


Figure 5. 4 Raman spectra of Co Mn-N-C/N-MC, Mn-N-C/N-MC, Co-N-C/N-MC

5.5 X-Ray Photoelectron Spectroscopy (XPS)

The elemental composition along with Bonding state of catalyst are determined using surface sensitive quantitative spectroscopic technique called XPS (X-ray photoelectron). To determine the surface composition and oxidation states involved in Co Mn-N-C/N-MC electrocatalyst XPS analysis was explored. XPS Survey spectra of obtained material were shown in figure 5.5 (a). It confirmed the presence of N, C, Mn and Co elements. Moreover, peaks of all element in spectrum were fitted by using a XPS fitting software, ‘XPSPEAK41’ [88]. Next in figure 5.5 (b) carbon (C1s) deconvoluted in 3 peaks of C=C, C-N and C=O with binding energy of 284.5, 285.5 and 286.1 [89]. The C1s signal at 285.6 eV, attributed to carbon atoms associating with N atoms, verifies the development of an N-doped framework of carbon [86]. Furthermore, the presence of C=C and C-N bonds indicates significant graphitization and effective N doping [90]. Figure 5.5 (c) The nitrogen (N1s) spectrum of Co Mn-N-C/N-MC revealed the presence of pyrrolic-N, pyridinic-N, graphitic-N, Metal-Nitride, oxidized-N at binding energies of 397.4, 400.5, 398.5, 399.2 and 401.5 respectively. According to published research, pyridinic nitrogen is especially useful for regulating the ORR's active sites. Graphitic N can serve as an electron donor to increase the catalytic activity of Pyridinic N for ORR also goes in favor

of OER. There are many active sites in graphitic and pyridinic N that allow O₂ molecules to dissolve and adsorb [43,44]. The electron density of nearby nitrogen-carbon sites may be impacted by localized charge redistribution within the carbon matrix caused by defective carbon structures. This change has the potential to greatly increase the oxygen reduction reaction's (ORR) activity [91]. Moreover Pyridinic and pyrrolic nitrogen are important for the formation of metal-nitrogen sites, while graphitic nitrogen may improve ORR performance, resulting in a synergistic impact and an increase in catalytic activity [92]. Apart from the two satellite peaks, two signals appear at 781.8 eV and 797.0 eV in the Co 2p spectrum, corresponding to the 2p_{3/2} and 2p_{1/2} peaks of Co²⁺, respectively. In contrast, the peaks observed at 779.8 eV and 794.9 eV are attributed to the 2p_{3/2} and 2p_{1/2} peaks of Co⁰, respectively [93]. The presence of Co⁰ enhances electron transfer to Mn-containing compounds, with this strong electronic interaction facilitating the adsorption and desorption of reaction intermediates (such as *O and *OOH) during oxygen electrocatalysis [94]. Similarly figure 5.5 (e) Three sub peaks of O1s spectrum formed which are centered at binding energies of 530.1eV, 531.3 eV and 532.3 eV and belongs to lattice OH, adsorbed water molecule and C=O. Figure 5.6 (f) shows F1s spectrum. Figure 5.7 (a) a peak in the XPS spectrum can be seen at 685 eV, which corresponds to manganese fluoride bonding energy, this signal is likely attributed to HF residue [95]. Additionally significant electrochemical activity has been shown by manganese fluoride in alkaline environments [96].

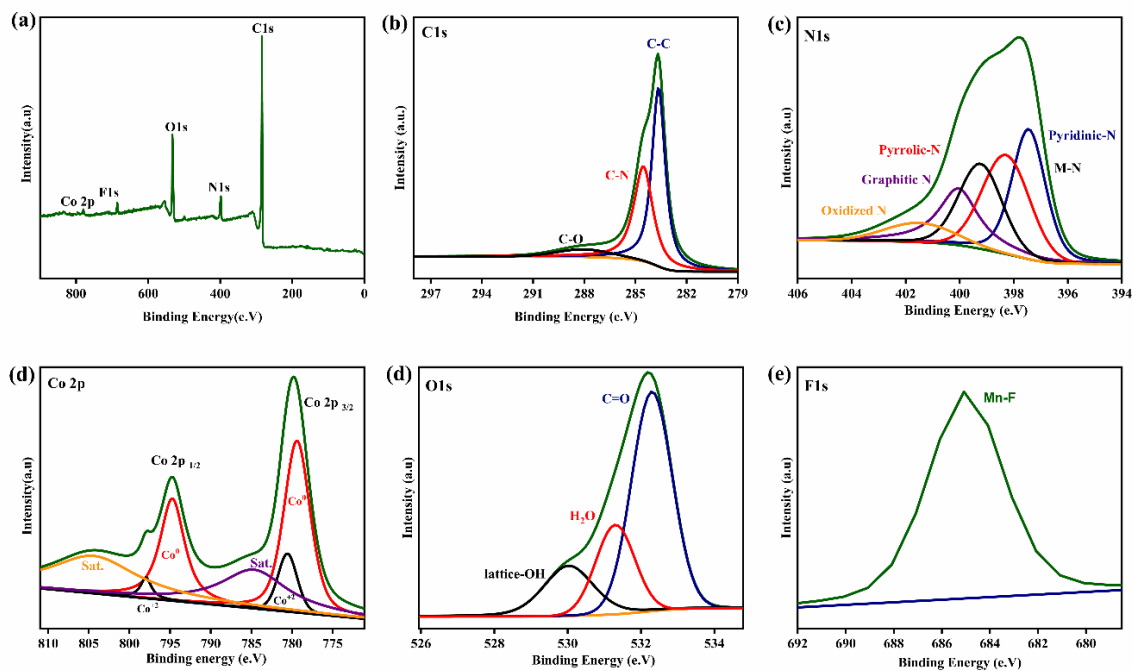


Figure 5.5 (a)XPS spectrum of Co Mn-N-C/N-MC (b) C1s (c) N1s (d)Co 2p (e) O1s (f) F1s

5.6 Linear Sweep Voltammetry (LSV)

5.6.1 Oxygen Reduction Reaction (ORR)

The ORR activities of single-atom and dual-atom electrocatalysts, including CoMn-N-C/N-MC, were evaluated through rotating disk electrode (RDE) analysis in a 0.1 M KOH solution. The electrode disc area was used to regulate current densities, ensuring accurate comparison across samples. Linear Sweep Voltammetry (LSV) results, presented in Figure 5.5 demonstrate that CoMn-N-C/N-MC exhibits the best ORR performance among the tested samples, including Co-N-C/N-MC, Mn-N-C/N-MC, and 20% Pt/C. The half-wave potential ($E_{1/2}$) for CoMn-N-C/N-MC is 0.85 V (vs. RHE), outperforming Co-N-C/N-MC, Mn-N-C/N-MC, and Pt/C by 37 mV, 28 mV, and 15 mV, respectively. Additionally, CoMn-N-C/N-MC displays an onset potential of 0.96 V (vs. RHE), which is nearly equivalent to 10% Pt/C (0.98 V) and superior to the monometallic catalysts (0.94 V). The enhanced ORR performance of CoMn-N-C/N-MC highlights the synergistic effect

of dual-atom sites, where the combination of pyridinic nitrogen and highly active Co and Mn sites results in improved catalytic activity and efficient atomic utilization.

Further analysis using the RDE system at varying rotational speeds (400–1600 rpm) reveals the impact of mass transfer on ORR kinetics. As seen in Figure 5.6 (b), the current density increases with rising rotation speeds, demonstrating that enhanced mass transfer accelerates the reaction rate. The rapid electron transfer associated with the improved reaction rate further raises the current density. The measured current density of 6.1 mA/cm² represents the combined contribution of kinetic current and mass diffusion current. To gain further insight into the reaction mechanism, Koutecky–Levich (K-L) plots were constructed for CoMn-N-C/N-MC, as shown in Figure 5.6 (c). These plots exhibit straight lines with slopes between 0 and 1, indicating that the kinetic factors dominate over mass transfer effects.

The number of electrons involved in the ORR was calculated from the K-L equation, and the results show that the average number of transferred electrons is close to 4. This confirms that the ORR on CoMn-N-C/N-MC follows a four-electron pathway, which is kinetically favorable and desirable for practical applications, as shown in Figure 5.6 (c). The ability of CoMn-N-C/N-MC to achieve efficient oxygen reduction through this pathway highlights its potential as a superior bifunctional catalyst for energy applications such as fuel cells and metal-air batteries

5.6.2 Oxygen Evolution reaction (OER)

We further investigated the Oxygen Evolution Reaction (OER) performance of the CoMn-N-C/N-MC electrocatalyst in a 0.1 M KOH solution. The results indicate that this electrocatalyst exhibits significant OER activity, demonstrating a low overpotential of 360 mV at a current density of 10 mA cm⁻². This performance is comparable to that of commercial RuO₂, but significantly superior to that of single-atom dispersed monometallic-N moieties. Notably, CoMn-N-C/N-MC showcases excellent OER activity relative to other samples in the study, contrasting with its previously discussed ORR performance figure 5.6 (d-e). The Tafel slope for CoMn-N-C/N-MC is measured at 55 mV

dec^{-1} (Table 1), which is considerably lower than that of RuO_2 (98 mV dec^{-1}), Co-N-C/N-MC (116 mV dec^{-1}), and Mn-N-C/N-MC (127 mV dec^{-1}). This low Tafel slope indicates fast OER kinetics, signifying that the CoMn-N-C/N-MC catalyst facilitates the OER process more efficiently than its counterparts.

To evaluate the overall performance of the oxygen electrode, we calculated the difference in potential (ΔE) between the OER potential at 10 mA cm^{-2} and the ORR half-wave potential. As shown in Figure 5.7 (f), the CoMn-N-C/N-MC electrocatalyst exhibits the smallest overpotential (ΔE) of approximately 0.74 V in the 0.1 M KOH solution, surpassing most transition metal-based bifunctional oxygen catalysts reported in the literature.

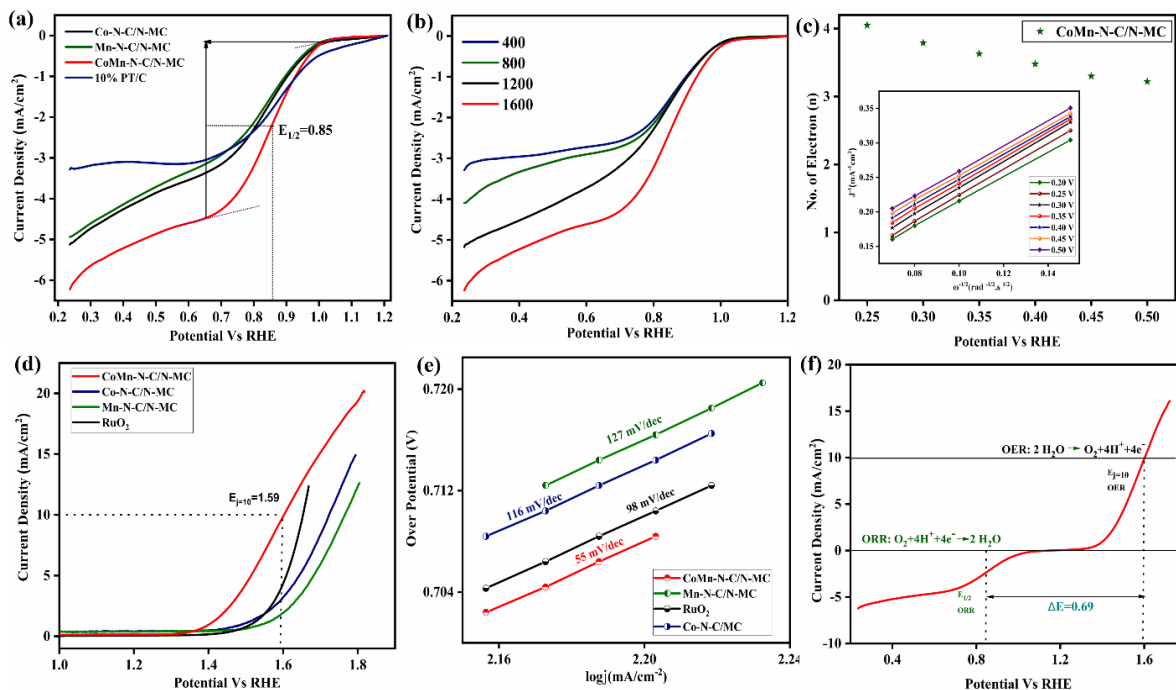


Figure 5. 6 (a) ORR of Co-N-C/N-MC , Co-N-C/N-MC , Co Mn-N-C/N-MC and $10\% \text{ Pt/C}$ (b) ORR at different rpm (c) K-L plots (d) OER plots Co-N-C/N-MC , Co-N-C/N-MC , Co Mn-N-C/N-MC and RuO_2 (e) Tafel plots (f) Combined ORR and OER overall LSV curves of Co Mn-N-C/N-MC

This exceptional performance underscores the potential of CoMn-N-C/N-MC as a highly effective bifunctional catalyst for both OER and ORR, making it a promising candidate for applications in energy conversion and storage systems. The synergistic effects arising from the dual-metal sites within the N-doped carbon framework contribute to the catalyst's enhanced efficiency and overall performance in electrochemical applications.

Table 5. 1 Electrochemical performance Prepared sample

Sample	Electrolyte	E_{onset}	Tafel slope	E_{=1/2}	Current Density	Over Potential
Co-N-C/N-MC	0.1 M KOH	0.98	116 mV/dec	0.819	5.1	0.67
Mn-N-C/N-MC	0.1 M KOH	0.94	127mV/dec	0.828	4.9	0.72
CoMn-N-C/N-MC	0.1 M KOH	0.96	55 mV/dev	0.856	6.1	0.36 V
Pt/C	0.1 M KOH	1.02	--	0.841	3.24	--
RuO ₂	0.1 M KOH	--	98 mV/dec	--	--	0.42 V

To evaluate the overall performance of the oxygen electrode, we calculated the difference in potential (ΔE) between the OER potential at 10 mA cm⁻² and the ORR half-wave potential. As shown in Figure 5.7 (f), the CoMn-N-C/N-MC electrocatalyst exhibits the smallest overpotential (ΔE) of approximately 0.74 V in the 0.1 M KOH solution, surpassing most transition metal-based bifunctional oxygen catalysts reported in the literature. This exceptional performance underscores the potential of CoMn-N-C/N-MC as a highly effective bifunctional catalyst for both OER and ORR, making it a promising candidate for applications in energy conversion and storage systems. The synergistic effects arising from the dual-metal sites within the N-doped carbon framework contribute

to the catalyst's enhanced efficiency and overall performance in electrochemical applications. Table 5.2 shows the comparison of different samples.

Table 5. 2 Comparison with Literature

Sample	$E_{1/2}$ V	E_{10} (V)	ΔE	Ref
Ni-N ₄ /GHSs/Fe-N ₄	0.83	1.62	0.79	[97]
CoNi-Sas/NC	0.76	1.57	0.81	[98]
FeCo-N-C	0.81	1.61	0.8	[3]
Fe-NSDC	0.84	1.61	0.80	[99]
Co-N, B-CSs	0.83	1.66	0.83	[100]
Pt/C and RuO ₂	0.84	1.65	-	This work
Co-N-C/N-MC	0.81	1.70	0.89	This work
Mn-N-C/N-MC	0.82	1.76	0.94	This work
CoMn-N-C/N-MC	0.85	1.59	0.74	This work

5.7 Stability Test

The durability of the sample is a critical factor when evaluating its potential for commercialization, as it directly impacts the long-term performance and reliability of the material [101]. To assess this aspect, we conducted long-term cycling tests on the sample. The results presented in Figure 5.7 demonstrate that there was only a minimal loss of activity after 1000 cycles, indicating a promising level of stability. Specifically, for the CoMn-N-C/N-MC electrocatalyst, we observed a negligible negative shift of 2.0 mV in the half-wave potential, suggesting that its electrochemical performance remains largely intact even after extensive cycling. Figure 5.7 (a) Furthermore, we evaluated the long-term stability of the CoMn-N-C/N-MC electrocatalyst in the context of oxygen evolution

reaction (OER) activity over the same 1000 cycles. As shown in Figure 5.7 (b), there was a modest decline of 8 mV in the potential required to achieve a current density of $E_j=10 \text{ mA cm}^{-2}$ by the end of the 1000th cycle figure 5.7 (b). This slight decrease in performance indicates that while the catalyst maintains a good level of stability, continuous monitoring and assessment are essential for understanding its long-term viability in practical applications.

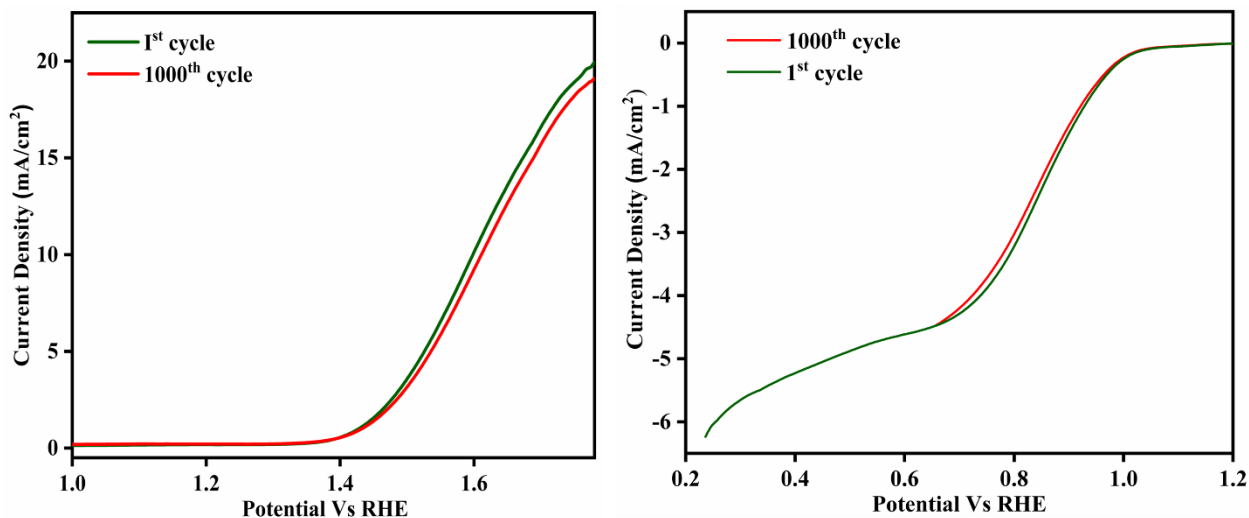


Figure 5. 7 Stability curve (a) OER and (b) ORR

5.8 Electrochemical Impedance Spectroscopy

Electrochemical Impedance Spectroscopy (EIS) was employed to further evaluate the electrochemical performance of the CoMn-N-C/N-MC catalyst, focusing on its impedance mechanism and charge transfer kinetics. The Nyquist plots, presented in Figure 5.8 consist of three distinct regions, each representing different electrochemical processes. The solution resistance (R_s), which accounts for the resistance of the electrolyte, is identified by the high-frequency intercept on the x-axis. The semicircle observed at high to medium frequencies reflects the charge transfer resistance (R_{ct}), representing the resistance encountered during electron transfer at the electrode-electrolyte interface. The linear segment at lower frequencies, known as the Warburg resistance (R_x), captures the diffusive behavior of ions within the porous electrode structure, indicating mass transport limitations [102]. To quantitatively assess the impedance behavior, the EIS data was fitted

using the CHI 760E software, employing an equivalent circuit model. A schematic of the equivalent circuit used for fitting is provided in the inset of Figure 5.8.

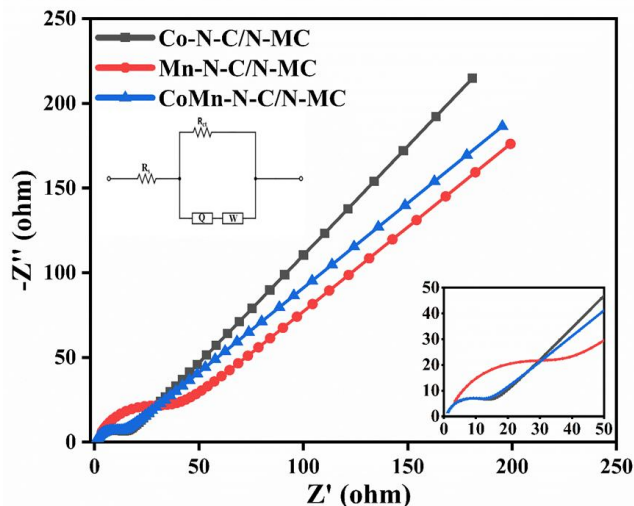


Figure 5. 8 EIS plots of Co-N-C/N-MC, Mn-N-C/N-MC and Co Mn-N-C/N-MC

The fitting allowed for accurate determination of key electrochemical parameters, such as R_t transport timings, all its output is represented in comprehensive time. Table 5.3 shows the Charge transfer resistance of each sample.

Table 5. 3 Charger transfer resistance of each sample

Material	R_s (Ω)	R_{ct} Ω
Mn-N-C/N-MC	0.001	23.16
Co-N-C/N-MC	0.002	11.98
CoMn-N-C/N-MC	0.14	8.36

The N-doped mesoporous carbon-supported CoMn-N-C/N-MC catalyst exhibits excellent bifunctional activity, significantly enhancing its performance for both the oxygen evolution reaction (OER) and the oxygen reduction reaction (ORR). The incorporation of

Co and Mn within the N-doped carbon matrix provides synergistic catalytic effects, improving the overall kinetics of both reactions. The high surface area and mesoporous structure of the carbon framework further contribute to the catalyst's efficiency by facilitating rapid oxygen transport to the active sites. The interconnected pores ensure better mass diffusion and improved accessibility of reactants, which is critical for sustaining high catalytic performance. This combination of enhanced active site exposure, fast charge transfer, and efficient oxygen transport underscores the potential of CoMn-N-C/N-MC as a promising material for Zinc-air batteries.

CHAPTER 6: CONCLUSION AND FUTURE RECOMMENDATION

6.1 Conclusion

CoMn-N-C/N-MC catalyst showcases remarkable performance as an efficient electrocatalyst for the oxygen evolution reaction (OER). Its low Tafel slope of 55.0 mV/dec indicates a rapid reaction rate, while the requirement of only 360 mV of overpotential at a current density of 10 mA/cm² signifies its high efficiency and energy-saving potential. This characteristic is particularly crucial in zinc air battery. Furthermore, the catalyst exhibits excellent stability, maintaining its electrocatalytic performance over extended periods. The outstanding performance and stability of CoMn-N-C/N-MC can be attributed to the presence of many active sites within its structure, facilitating the efficient flow of charges and electrons during electrochemical reactions. The unique properties of the metal atom catalyst contribute significantly to enhancing the overall electrocatalytic activity. The synergistic effect arising from the combination of the active sites and the metal atom catalyst leads to improved charge transfer kinetics and faster electron transport during the electrochemical reaction. Overall, the findings of this study underscore the potential of CoMn-N-C/N-MC as a leading candidate for practical applications in energy conversion and storage technologies.

6.2 Future Recommendation

Refining the synthesis process is crucial to improving the morphology, surface area, and metal distribution of electrocatalysts, leading to enhanced catalytic efficiency. Additionally, exploring new metal combinations and investigating their interactions can uncover synergies that improve both activity and stability. Furthermore, evaluating catalyst performance in alternative applications, such as water splitting for hydrogen production and supercapacitors for energy storage, can provide valuable insights into their versatility. Testing these catalysts in diverse applications will help establish their potential for broader renewable energy use.

REFERENCES

1. Martins, F., et al. Analysis of Fossil Fuel Energy Consumption and Environmental Impacts in European Countries. *Energies*, 2019. **12**, DOI: 10.3390/en12060964.
2. Al Mubarak, F., R. Rezaee, and D.A. Wood, Economic, Societal, and Environmental Impacts of Available Energy Sources: A Review. *Eng*, 2024. **5(3)**: p. 1232-1265.
3. Dehghani-Sanij, A.R., et al., Study of energy storage systems and environmental challenges of batteries. *Renewable and Sustainable Energy Reviews*, 2019. **104**: p. 192-208.
4. Al-Ghussain, L., Global warming: review on driving forces and mitigation. *Environmental Progress & Sustainable Energy*, 2019. **38(1)**: p. 13-21.
5. Kalair, A., et al., Role of energy storage systems in energy transition from fossil fuels to renewables. *Energy Storage*, 2021. **3(1)**: p. e135.
6. Khan, N., et al., Review of energy storage and transportation of energy. *Energy Storage*, 2019. **1(3)**: p. e49.
7. Zhang, C., et al., Energy storage system: Current studies on batteries and power condition system. *Renewable and Sustainable Energy Reviews*, 2018. **82**: p. 3091-3106.
8. Yang, Y., et al., Battery energy storage system size determination in renewable energy systems: A review. *Renewable and Sustainable Energy Reviews*, 2018. **91**: p. 109-125.
9. Jose, T., et al., Elastomeric polymer blend nanocomposites for energy storage applications, in *Polymer Blend Nanocomposites for Energy Storage Applications*. 2023, Elsevier. p. 91-107.
10. Olabi, A.G., et al., Metal-air batteries—a review. *Energies*, 2021. **14(21)**: p. 7373.
11. Liu, Q., et al., Aqueous metal-air batteries: Fundamentals and applications. *Energy Storage Materials*, 2020. **27**: p. 478-505.
12. Aasen, D., M.P. Clark, and D.G. Ivey, Investigation of transition metal-based (Mn, Co, Ni, Fe) trimetallic oxide nanoparticles on n-doped carbon nanotubes as bifunctional catalysts for zn-air batteries. *Journal of The Electrochemical Society*, 2020. **167(4)**: p. 040503.
13. Li, X., et al., Active sites identification and engineering of MNC electrocatalysts toward oxygen reduction reaction. *International Journal of Hydrogen Energy*, 2024. **51**: p. 1110-1127.

14. Tang, T., Z. Wang, and J. Guan, Electronic structure regulation of single-site MNC electrocatalysts for carbon dioxide reduction. *Acta Phys.–Chim. Sin.*, 2022. **39**: p. 10-3866.
15. Mitali, J., S. Dhinakaran, and A. Mohamad, Energy storage systems: A review. *Energy Storage and Saving*, 2022. **1**(3): p. 166-216.
16. Paloheimo, H. and M. Omidiora. A feasibility study on Compressed Air Energy Storage system for portable electrical and electronic devices. in 2009 International Conference on Clean Electrical Power. 2009. IEEE.
17. Ahmed, A., et al., Hydrogen fuel and transport system: A sustainable and environmental future. *International journal of hydrogen energy*, 2016. **41**(3): p. 1369-1380.
18. Buttner, W.J., et al., An overview of hydrogen safety sensors and requirements. *International Journal of Hydrogen Energy*, 2011. **36**(3): p. 2462-2470.
19. Züttel, A., Hydrogen storage methods. *Naturwissenschaften*, 2004. **91**: p. 157-172.
20. Duan, J., et al., Building safe lithium-ion batteries for electric vehicles: a review. *Electrochemical Energy Reviews*, 2020. **3**: p. 1-42.
21. Yaqoob, L., T. Noor, and N. Iqbal, An overview of metal-air batteries, current progress, and future perspectives. *Journal of Energy Storage*, 2022. **56**: p. 106075.
22. Li, M., et al., Relating catalysis between fuel cell and metal-air batteries. *Matter*, 2020. **2**(1): p. 32-49.
23. Yu, D., et al., Dual-sites coordination engineering of single atom catalysts for flexible metal–air batteries. *Advanced Energy Materials*, 2021. **11**(30): p. 2101242.
24. Liang, Z., et al., Metal-organic framework-derived materials for electrochemical energy applications. *EnergyChem*, 2019. **1**(1): p. 100001.
25. Liu, A., et al., Recent progress in MXene-based materials for metal-sulfur and metal-air batteries: potential high-performance electrodes. *Electrochemical Energy Reviews*, 2022: p. 1-33.
26. Fan, X.-Z., et al., In situ construction of bifunctional N-doped carbon-anchored Co nanoparticles for OER and ORR. *ACS Applied Materials & Interfaces*, 2022. **14**(6): p. 8549-8556.
27. Wang, L., et al., Sustainable aqueous metal-air batteries: An insight into electrolyte system. *Energy Storage Materials*, 2022. **52**: p. 573-597.

28. Deyab, M. and Q. Mohsen, Improved battery capacity and cycle life in iron-air batteries with ionic liquid. *Renewable and Sustainable Energy Reviews*, 2021. **139**: p. 110729.
29. Liu, T., et al., Current challenges and routes forward for nonaqueous lithium–air batteries. *Chemical Reviews*, 2020. **120**(14): p. 6558-6625.
30. Suryatna, A., et al., A Review of High-Energy Density Lithium-Air Battery Technology: Investigating the Effect of Oxides and Nanocatalysts. *Journal of Chemistry*, 2022. **2022**(1): p. 2762647.
31. Li, H., J. Chen, and J. Fang, Recent advances in wearable aqueous metal-air batteries: From configuration design to materials fabrication. *Advanced Materials Technologies*, 2023. **8**(8): p. 2201762.
32. Bi, X., et al., Rechargeable zinc–air versus lithium–air battery: from fundamental promises toward technological potentials. *Advanced Energy Materials*, 2024. **14**(6): p. 2302388.
33. Wu, P., et al., Modification on water electrochemical environment for durable Al-Air Battery: Achieved by a Low-Cost sucrose additive. *Chemical Engineering Journal*, 2022. **438**: p. 135538.
34. Zhang, S., et al., Advanced noncarbon materials as catalyst supports and non-noble electrocatalysts for fuel cells and metal–air batteries. *Electrochemical Energy Reviews*, 2021. **4**: p. 336-381.
35. Zhang, H., et al., Doping engineering: modulating the intrinsic activity of bifunctional carbon-based oxygen electrocatalysts for high-performance zinc–air batteries. *Journal of Materials Chemistry A*, 2022. **10**(41): p. 21797-21815.
36. Müller, S., F. Holzer, and O. Haas, Optimized zinc electrode for the rechargeable zinc–air battery. *Journal of applied electrochemistry*, 1998. **28**: p. 895-898.
37. Caramia, V. and B. Bozzini, Materials science aspects of zinc–air batteries: a review. *Materials for Renewable and Sustainable Energy*, 2014. **3**: p. 1-12.
38. Caparrós, J.J., et al., Optimized Balance of Plant for a Medium-size PEM electrolyzer. *Design, Modelling and Control. Simul. Notes Eur.*, 2021. **31**(3): p. 133-141.
39. Saha, P., et al., Cobalt Oxide-Based Electrocatalysts with Bifunctionality for High-Performing Rechargeable Zinc-Air Batteries. *The Chemical Record*, 2024. **24**(1): p. e202300216.
40. Wang, Y., et al., Advanced electrocatalysts with single-metal-atom active sites. *Chemical reviews*, 2020. **120**(21): p. 12217-12314.

41. Zhang, H., et al., Catalysis of a single transition metal site for water oxidation: from mononuclear molecules to single atoms. *Advanced Materials*, 2020. **32**(18): p. 1904037.
42. Ma, Y., et al., An efficient dual-metal single-atom catalyst for bifunctional catalysis in zinc-air batteries. *Carbon*, 2021. **185**: p. 526-535.
43. Dey, G., et al., Dual single-atomic Co–Mn sites in metal–organic-framework-derived N-doped nanoporous carbon for electrochemical oxygen reduction. *ACS nano*, 2023. **17**(19): p. 19155-19167.
44. Liu, P., et al., Surface coordination chemistry of metal nanomaterials. *Journal of the American Chemical Society*, 2017. **139**(6): p. 2122-2131.
45. Maschmeyer, T., et al., Heterogeneous catalysts obtained by grafting metallocene complexes onto mesoporous silica. *Nature*, 1995. **378**(6553): p. 159-162.
46. Lang, R., et al., Single-atom catalysts based on the metal–oxide interaction. *Chemical reviews*, 2020. **120**(21): p. 11986-12043.
47. Guo, J., et al., A minireview on the synthesis of single atom catalysts. *RSC advances*, 2022. **12**(15): p. 9373-9394.
48. Zhang, W., et al., Emerging dual-atomic-site catalysts for efficient energy catalysis. *Advanced Materials*, 2021. **33**(36): p. 2102576.
49. Li, L., K. Yuan, and Y. Chen, Breaking the scaling relationship limit: from single-atom to dual-atom catalysts. *Accounts of Materials Research*, 2022. **3**(6): p. 584-596.
50. Chen, Y., et al., Single-atom catalysts: synthetic strategies and electrochemical applications. *Joule*, 2018. **2**(7): p. 1242-1264.
51. Liu, H., et al., Dual-atom active sites embedded in two-dimensional C₂N for efficient CO₂ electroreduction: A computational study. *Journal of Energy Chemistry*, 2021. **61**: p. 507-516.
52. He, T., et al., Atomically dispersed heteronuclear dual-atom catalysts: A new rising star in atomic catalysis. *Small*, 2022. **18**(12): p. 2106091.
53. Xie, P., et al., Oxo dicopper anchored on carbon nitride for selective oxidation of methane. *Nature Communications*, 2022. **13**(1): p. 1375.
54. Tran, M.-K., et al. A Review of Range Extenders in Battery Electric Vehicles: Current Progress and Future Perspectives. *World Electric Vehicle Journal*, 2021. **12**, DOI: 10.3390/wevj12020054.

55. Gao, C., et al., Recent Advances in ZIF-Derived Atomic Metal–N–C Electrocatalysts for Oxygen Reduction Reaction: Synthetic Strategies, Active Centers, and Stabilities. *Small*, 2022. **18**(14): p. 2105409.
56. Wang, S., et al., Recent advances in tailoring zeolitic imidazolate frameworks (ZIFs) and their derived materials based on hard template strategy for multifunctional applications. *Coordination Chemistry Reviews*, 2024. **498**: p. 215464.
57. Arafat, Y., et al., Advances in Zeolite Imidazolate Frameworks (ZIFs) Derived Bifunctional Oxygen Electrocatalysts and Their Application in Zinc–Air Batteries. *Advanced Energy Materials*, 2021. **11**(26): p. 2100514.
58. Kong, Q.-H., et al., Curving Engineering of Hollow Concave-Shaped Rhombic Dodecahedrons of N-Doped Carbon Encapsulated with Fe-Doped Co/Co₃O₄ Nanoparticles for an Efficient Oxygen Reduction Reaction and Zn–Air Batteries. *ACS Sustainable Chemistry & Engineering*, 2022. **10**(34): p. 11441-11450.
59. Wu, J., et al., Densely Populated Isolated Single Co–N Site for Efficient Oxygen Electrocatalysis. *Advanced Energy Materials*, 2019. **9**(22): p. 1900149.
60. Xie, A., et al., Elaborate construction of honeycomb-like porous carbon with embedment of N-doped carbon nanotubes as efficient electrocatalyst for zinc-air battery. *Carbon*, 2024. **228**: p. 119299.
61. Xie, W.W., et al., Formation of hollow frameworks of dual-sided Fe/Fe₃C@N-doped carbon nanotubes as bifunctional oxygen electrocatalyst for Zn-air batteries. *Applied Catalysis B: Environmental*, 2022. **317**: p. 121760.
62. Sheng, J., et al., Carbon nanotube supported bifunctional electrocatalysts containing iron-nitrogen-carbon active sites for zinc-air batteries. *Nano Research*, 2021. **14**(12): p. 4541-4547.
63. Zahra, K., et al., A review on the modification strategies of transition metal based bifunctional electrocatalysts for air-cathode in zinc-air batteries. *Journal of Energy Storage*, 2024. **88**: p. 111565.
64. Cheng, J., et al., Steering the oxygen reduction reaction pathways of N-carbon hollow spheres by heteroatom doping. *Applied Catalysis B: Environmental*, 2023. **327**: p. 122470.
65. Wu, L., et al., High-Efficiency Oxygen Evolution Reaction: Controllable Reconstruction of Surface Interface. *Small*, 2023. **19**(49): p. 2304007.
66. Dong, F., et al., Atomically Dispersed Transition Metal-Nitrogen-Carbon Bifunctional Oxygen Electrocatalysts for Zinc-Air Batteries: Recent Advances and Future Perspectives. *Nano-Micro Letters*, 2021. **14**(1): p. 36.

67. Sun, H., et al., Updating the Intrinsic Activity of a Single-Atom Site with a P–O Bond for a Rechargeable Zn–Air Battery. *ACS Applied Materials & Interfaces*, 2019. **11**(36): p. 33054-33061.
68. Wei, L., et al., Recent advances of transition metal based bifunctional electrocatalysts for rechargeable zinc-air batteries. *Journal of Power Sources*, 2020. **477**: p. 228696.
69. Wang, J., et al., Structure-Performance Descriptors and the Role of the Axial Oxygen Atom on M–N₄–C Single-Atom Catalysts for Electrochemical CO₂ Reduction. *ACS Catalysis*, 2022. **12**(9): p. 5441-5454.
70. Musa, E., F. Doherty, and B.R. Goldsmith, Accelerating the structure search of catalysts with machine learning. *Current Opinion in Chemical Engineering*, 2022. **35**: p. 100771.
71. Cheng, W., et al., Boosting defective carbon by anchoring well-defined atomically dispersed metal-N₄ sites for ORR, OER, and Zn-air batteries. *Applied Catalysis B: Environmental*, 2020. **260**: p. 118198.
72. Ali, A.S., Application of nanomaterials in environmental improvement. *Nanotechnology and the Environment*, 2020: p. 17-36.
73. Gosser, D.K., Cyclic voltammetry: simulation and analysis of reaction mechanisms. Vol. 43. 1993: VCH New York.
74. Marken, F., A. Neudeck, and A.M. Bond, Cyclic voltammetry. *Electroanalytical methods: guide to experiments and applications*, 2010: p. 57-106.
75. Rossmeisl, J., et al., Steady state oxygen reduction and cyclic voltammetry. *Faraday discussions*, 2009. **140**: p. 337-346.
76. Kristoffersen, H.H., T. Vegge, and H.A. Hansen, OH formation and H₂ adsorption at the liquid water–Pt (111) interface. *Chemical science*, 2018. **9**(34): p. 6912-6921.
77. Prass, S., et al., Hydrogen oxidation artifact during platinum oxide reduction in cyclic voltammetry analysis of low-loaded PEMFC electrodes. *Electrocatalysis*, 2021. **12**: p. 45-55.
78. Koper, M.T., Introductory Lecture Electrocatalysis: theory and experiment at the interface. *Faraday Discussions*, 2009. **140**: p. 11-24.
79. Stephens, I.E., et al., Understanding the electrocatalysis of oxygen reduction on platinum and its alloys. *Energy & Environmental Science*, 2012. **5**(5): p. 6744-6762.
80. Xing, W., G. Yin, and J. Zhang, Rotating electrode methods and oxygen reduction electrocatalysts. 2014: Elsevier.

81. Chen, W., et al., Reconsidering the benchmarking evaluation of catalytic activity in oxygen reduction reaction. *IScience*, 2020. **23**(10).
82. Han, X., et al., Application of the electrochemical oxygen reduction reaction (ORR) in organic synthesis. *Advanced Synthesis & Catalysis*, 2019. **361**(12): p. 2804-2824.
83. Kuang, F., et al., Electrochemical impedance spectroscopy analysis for oxygen reduction reaction in 3.5% NaCl solution. *Journal of Solid State Electrochemistry*, 2009. **13**: p. 385-390.
84. Chang, B.-Y. and S.-M. Park, Electrochemical impedance spectroscopy. *Annual Review of Analytical Chemistry*, 2010. **3**(1): p. 207-229.
85. Raistrick, I.D., Application of impedance spectroscopy to materials science. *Annual Review of Materials Science*, 1986. **16**(1): p. 343-370.
86. Han, J., et al., 3D N-doped ordered mesoporous carbon supported single-atom Fe-NC catalysts with superior performance for oxygen reduction reaction and zinc-air battery. *Applied Catalysis B: Environmental*, 2021. **280**: p. 119411.
87. Han, J., et al., Single-atom Fe-N_x-C as an efficient electrocatalyst for zinc-air batteries. *Advanced Functional Materials*, 2019. **29**(41): p. 1808872.
88. PSpak 41 is a free software, available from rmkwok@cuhk.edu.hk.
89. Chen, X., X. Wang, and D. Fang, A review on C1s XPS-spectra for some kinds of carbon materials. *Fullerenes, Nanotubes and Carbon Nanostructures*, 2020. **28**(12): p. 1048-1058.
90. Zhang, F., et al., Template-assisted polymerization-pyrolysis derived mesoporous carbon anchored with Fe/Fe₃C and Fe-N_x species as efficient oxygen reduction catalysts for Zn-air battery. *International Journal of Hydrogen Energy*, 2021. **46**(76): p. 37895-37906.
91. Ding, J., et al., The synthesis of MOF derived carbon and its application in water treatment. *Nano Research*, 2022. **15**(8): p. 6793-6818.
92. Zhang, J., et al., Defect and pyridinic nitrogen engineering of carbon-based metal-free nanomaterial toward oxygen reduction. *Nano Energy*, 2018. **52**: p. 307-314.
93. Zhao, C., et al., A Co-Fe Prussian blue analogue for efficient Fenton-like catalysis: the effect of high-spin cobalt. *Chemical Communications*, 2019. **55**(50): p. 7151-7154.
94. Lu, X.F., et al., Interfacing manganese oxide and cobalt in porous graphitic carbon polyhedrons boosts oxygen electrocatalysis for Zn-air batteries. *Advanced Materials*, 2019. **31**(39): p. 1902339.

95. Zukiene, K., et al., Wettability of MXene and its interfacial adhesion with epoxy resin. *Materials Chemistry and Physics*, 2021. **257**: p. 123820.
96. He, Z.-H., J.-F. Gao, and L.-B. Kong, Electrolyte effect on electrochemical behaviors of manganese fluoride material for aqueous asymmetric and symmetric supercapacitors. *Rare Metals*, 2024. **43**(3): p. 1048-1061.
97. Chen, J., et al., Dual single-atomic Ni-N₄ and Fe-N₄ sites constructing Janus hollow graphene for selective oxygen electrocatalysis. *Advanced Materials*, 2020. **32**(30): p. 2003134.
98. Han, X., et al., Atomically dispersed binary Co-Ni sites in nitrogen-doped hollow carbon nanocubes for reversible oxygen reduction and evolution. *Advanced Materials*, 2019. **31**(49): p. 1905622.
99. Zhang, J., et al., Single Fe atom on hierarchically porous S, N-codoped nanocarbon derived from porphyrin enable boosted oxygen catalysis for rechargeable Zn-air batteries. *Small*, 2019. **15**(24): p. 1900307.
100. Guo, Y., et al., Carbon nanosheets containing discrete Co-N_xB_yC active sites for efficient oxygen electrocatalysis and rechargeable Zn–Air batteries. *ACS nano*, 2018. **12**(2): p. 1894-1901.
101. Wang, B., et al., Space-confined yolk-shell construction of Fe₃O₄ nanoparticles inside N-doped hollow mesoporous carbon spheres as bifunctional electrocatalysts for long-term rechargeable zinc–air batteries. *Advanced Functional Materials*, 2020. **30**(51): p. 2005834.
102. Chen, L.-F., et al., Designed formation of hollow particle-based nitrogen-doped carbon nanofibers for high-performance supercapacitors. *Energy & Environmental Science*, 2017. **10**(8): p. 1777-1783.

LIST OF PUBLICATIONS

em Journal of Electroanalytical Chemistry						
Home	Main Menu	Submit a Manuscript	About ▾	Help ▾		
← Submissions Being Processed for Author ⓘ						
Page: 1 of 1 (1 total submissions)				Results per page 10 ▾		
Action	Manuscript Number	Title	Authorship	Initial Date Submitted	Status Date	Current Status
Action Links	JELECHEM-D-24-02934	N-doped mesoporous carbon supported Dual-metal atom M-N-C desert rose structure for oxygen electrode electrocatalyst in zinc air battery	Other Author	Nov 20, 2024	Nov 27, 2024	Under Review